Available online at www.sciencedirect.com

ScienceDirect

Advances in Space Research 67 (2021) 2416–2438

ADVANCES IN SPACE RESEARCH (a COSPAR publication)

www.elsevier.com/locate/asr

Ground and satellite-based observations of ionospheric plasma bubbles and blobs at 5.65° latitude in the Brazilian sector

Ebenezer Agyei-Yeboah [a,*], Paulo Roberto Fagundes [a], Alexandre Tardelli [a], Valdir Gil Pillat [a], Alessio Pignalberi [b], Venkatesh Kavutarapu [c], Michael Pezzopane [b] Francisco Vieira [a,d]

[a] Laboratorio de Física e Astronomia, Universidade do Vale do Paraiba (UNIVAP), Av Shishima Hifumi, 2911, Urbanova, 12244-000, Sao Jose dos Campos, SP, Brazil

[b] Istituto Nazionale di Geofisica e Vulcanologia, Via di Vigna Murata, 605, 00143 Rome, Italy

[c] National Atmospheric Research Laboratory (NARL), Gadanki, India

[d] Observatório de Física Espacial, Instituto Federal de Tocantins-IFTO, Araguatins, Rua Castelo Branco, Brazil, Povoado Santa Tereza-km 05, Brazil

Received 30 September 2020; received in revised form 14 January 2021; accepted 18 January 2021
Available online 4 February 2021

Abstract

This investigation uses simultaneous observations from all-sky imager system and an ionosonde collocated at Araguatins (5.65° S, 48.07° W and dip-latitude of 4.17° S), a near-equatorial region in Brazil. These simultaneous observations were used to investigate the occurrence of plasma bubbles and blobs in the field of the imaging system and their association with atypical range Spread-F signature in ionograms. Also, in-situ observation of plasma density from Swarm satellites were used to support the ground-based observations. Using a few cases, a methodology will be established to identify in the plasma blobs (atypical ESF) in the ionograms when there is the simultaneous observation of plasma bubbles and blobs in the field of view of the ionosonde. For this purpose, simultaneous sequence of OI 630.0 nm nightglow images and ionograms are presented for different case studies; 1. when there is the absence of a plasma bubble or blob, 2. when there is only the occurrence of plasma bubbles and 3. when there is the occurrence of plasma bubbles and blobs, in order to compare traces in the ionogram in all these case studies. With these we can cover all kinds of signatures in the ionograms corresponding to no irregularities, plasma bubbles only and plasma bubbles-blobs. These OI 630.0 nm nightglow and ionograms recorded simultaneously make it possible to establish a novel methodology to recognize in ionograms cases when there is the occurrence of Spread-F signature associated with bubble-blob in the FOV of the ionosonde.

Keywords: Plasma bubbles; Plasma blobs; Spread-F; Equatorial Ionization Anomaly; Prereversal enhancement

1. Introduction

Large-scale equatorial ionospheric irregularities are regions of plasma depletions which are almost aligned to the Earth's magnetic field (covering the low latitudes in both hemispheres including the equatorial region). These depletions are generated after sunset or during the nighttime and are characterized by having a plasma density lower than the background ionospheric plasma (Mendillo and Baumgardner, 1982). On the other hand, blobs are regions where the plasma density is larger than the ambient ionospheric plasma (Pimenta et al., 2004).

The occurrence of plasma bubbles and blobs has been studied with techniques like GPS (Cherniak and Zakharenkova, 2016; Kumar, 2017), imaging systems

* Corresponding author.
E-mail address: agyeiyeboah.e@univap.br (E. Agyei-Yeboah).

https://doi.org/10.1016/j.asr.2021.01.034
0273-1177/

(Sahai et al., 2000; Sobral et al., 2002; Pimenta et al., 2004) and in-situ or satellite techniques (Oya et al., 1986; McNamara et al., 2013; Huang et al., 2014; Park et al., 2003; Park et al., 2015; Xiong et al., 2018) in different local time (LT) sectors. After the first observations of blobs by Oya et al. (1986) and Watanabe and Oya (1986), various authors have studied the occurrence of plasma blobs either independently or accompanied by plasma bubbles using satellite, radar or optical techniques (Park et al., 2003; Pimenta et al., 2004, 2007; Tardelli-Coelho et al., 2017; Kil et al., 2011, 2019; Wang et al., 2019).

The generation and source of plasma blobs are currently topics of considerable discussion in the research community. Researchers like Le et al. (2003), Pimenta et al. (2004, 2007) claim that plasma blobs occur simultaneously with plasma bubbles and that plasma bubbles could be a potential source for the generation of blobs. On the contrary, Miller et al. (2014) and Kil et al. (2019) have suggested medium-scale traveling ionospheric disturbances (MSTIDs) as possible source for plasma blob generation. Recently, gravity waves (GWs) were suggested also as potential source for plasma blobs in a paper published Wang et al., in 2019. Again, Kil et al. (2011) reported the occurrence of blobs in locations where plasma bubbles were reportedly absent, and suggested that plasma bubbles may not necessarily be a prerequisite condition for the generation of plasma blobs and that they could occur independently from plasma bubbles.

Pimenta et al. (2004, 2007) and Tardelli-Coelho et al. (2017) using nightglow imaging techniques in the Brazilian sector, reported the observation of plasma blobs occurring in the company of plasma bubbles in the same longitude sectors. Also, from simultaneous observations of backscatter plumes and blobs, Yokoyama et al. (2007) proposed that there is a causal linkage between bubbles and blobs. Huang et al. (2014) observed plasma enhancements associated with plasma bubbles from ion density measurements by the planar Langmuir probe (PLP) onboard the Communication/Navigation Outage Forecasting System (C/NOFS) satellite and proposed a unified explanation for the relationship between plasma bubbles and blobs. They explained that blobs occur at any altitude or latitude in the ionosphere during the lifetime of plasma bubbles and that in the initial phase, Rayleigh-Taylor instability growth, and $\vec{E}x\vec{B}$ drift from polarization electric field lifts the F-layer causing plasma enhancement in the topside of the F-layer. Accordingly, plasma enhancements occur at the upper boundary of the depletion layer when they reach the topside and at latter stages, depletions are observed at the equator while enhancements are observed at higher latitudes of the same longitude. Furthermore, Le et al. (2003) have suggested that plasma enhancements (blobs) are generated by polarization electric fields which are produced in plasma density depletions which can be mapped to the anomaly regions along the magnetic field lines. Model simulations showed that it is possible to produce plasma bubbles together with plasma blobs at or above the Equatorial Ionospheric Anomaly (EIA) region (Krall et al., 2010).

The observation of plasma blobs and their association to ionosonde measurements has not been studied much. However, Fagundes et al. (2012) observed "atypical" range Spread-F features in ionograms from Sao Jose dos Campos (23.21°S,45.97°W) and Cachoeira Paulista (22.70°S, 45.01°W) in Brazil. According to them, these atypical structures are not a consequence of equatorial plasma bubbles or blobs (EPBs) originating from the southern crest of the EIA. These features which were observed to be beyond the background critical frequency of the typical ESF trace were at or above the virtual height of the F-layer and were related to MSTIDs (Fagundes et al., 2012). Pimenta et al. (2004, 2007) studying all-sky images and ionograms reported higher frequencies in the ionosonde measurements corresponding to increases in plasma density when plasma blobs appeared in the nightglow images. They reported that these measurements associated with blobs were well beyond the F_2-layer critical frequency (*fo*F2). Narayanan et al. (2014) also observed in ionograms similar traces at higher frequencies corresponding to plasma blobs and explained that it is possible to notice corresponding signatures of enhanced electron density regions in ionograms between depletions (Spread-F) since the field of view of the ionosonde is large enough to capture both phenomena. They specified that the reflections due to these irregularities must be higher than *fo*F2 and could be observed between adjacent plasma depletions. In the Asian-Oceanian sector, three cases of plasma blobs were observed by ROCSAT-1 satellite with simultaneous observations from ionosondes showing extra traces observed beyond the *fo*F2, resulting from the plasma blobs (Wang et al., 2019).

Calvert and Cohen, (1961) reported on their investigation on equatorial Spread-F (ESF) echo characteristics in ionograms and concluded that the main features of equatorial Spread-F echoes as observed in ionograms depend on scattering irregularities and their horizontal distribution with respect to the ionosonde. They showed various scenarios of ionogram features corresponding to different scattering irregularities and their location viz a viz location of the ionosonde. The Spread-F (SF) configuration observed in ionograms, associated with plasma blobs, presented in this paper and the aforementioned works (Pimenta et al., 2004; 2007; Narayanan et al., 2014; Wang et al., 2019) are similar to some of the configurations investigated by Calvert and Cohen, (1961).

In this paper, we present simultaneous ground-based observations of plasma bubbles (plasma depletion) and blobs (plasma enhancement) using the OI 630.0 nm nightglow emission images and ionograms carried out using an all-sky imager system and ionosonde, respectively. These instruments are located at the Araguatins (5.65° S, 48.07° W, and dip-latitude of 4.17° S, hereafter ARA) observatory. The occurrence of bubbles and blobs in the OI 630.0 nm emission nightglow images were observed simultaneously with the signature of the atypical range SF iono-

grams. We present and discuss the comparison between the OI 630.0 nm nightglow emission images with bubbles and blobs and their corresponding ionograms and propose a novel methodology to identify this kind of atypical ionograms by taking advantage of the unique collocation of the ground-based instruments and the simultaneous observations. This will allow for the study of plasma bubbles and blobs in the absence of an imaging system. It will also make it possible to study these irregularities at all times and seasons since the ionosonde does not have the weather (cloud) and moonlight condition limitations imposed on imaging systems. In-situ latitudinal electron density measurements observed by Swarm satellites were used as complementary data whenever possible to cross-check our ground-based observations. The results are presented case-by-case (night-by-night) allowing for comparison among the three techniques employed in the study.

2. Instruments and methods

An all-sky imaging (ASI) system, designed and constructed by KEO Scientific LTD, has been used to observe the OI 630.0 nm nightglow to study the ionosphere and to observe equatorial plasma bubbles, blobs and other ionospheric irregularities in the Brazilian sector (Sahai et al., 2000; Sobral et al., 2002; Pimenta et al., 2004; Paulino et al., 2010). In 2017, an all-sky imaging of OI630.0 nm nightglow emission was carried out at the observation site in ARA (5.65° S, 48.07° W and dip-latitude of 4.17° S), Brazil (Fig. 1). The imaging system comprises a fisheye lens with high spatial resolution and a field of view (FOV) of 180°, a telecentric lens, a six-position filter wheel of interference filters, a re-imaging system, a charge-coupled device detector of 2,048 × 2,048 pixels with a pixel depth of 16 bits, a cooling system responsible for minimizing the thermal noise of the camera and a computer. Rays passing through the fisheye lens are collimated at right-angles and parallel to each other pass through the filters. The imager has 4-inch diameter interference filters. The filter wheel holds the background, sky lenses and the OI630 nm, OI557.7 nm OI777.4 nm filters. This system can make quantitative measurements with high quantum efficiency, low thermal noise, low readout noise and high linearity. The microcomputer connected to the system is used for the control of the filter wheel and the data acquisition sequence. The OI630.0 nm nightglow emission images used in this study were recorded at intervals of 3–4 min considering the operation sequence and the number of filters used.

The all-sky imaging system can capture and characterizing the morphology of plasma bubbles and blobs over wide regions of the sky (for example, at 250 km altitude, 75° zenith angle - Z.A., the FOV of the ASI is approximately 1800 km in diameter – see Fig. 1). Because of the specific geometric configuration of the geographic and geomagnetic equators in the Brazilian sector (See Fig. 1), the all-sky imaging system operated at ARA can observe the spatial–temporal variation of the OI 630 nm nightglow emission intensity from southern hemisphere low-latitude, equatorial regions and northern hemisphere low-latitude (from 10°N to 20°S). This makes it a particularly important technique in ionospheric probing, especially for the study of plasma irregularities in the equatorial and low latitude regions. The OI630.0 nm nightglow emission line which is produced at the bottom side of the F-region at ~ 250–270 km altitude, offers a means to study remotely the ionospheric plasma and its variations in space and time. The emission line from oxygen gives information about the dynamical processes occurring in the ionospheric F-region, example the plasma density at that altitude. During the nighttime, the OI630.0 nm emission line is produced by dissociative recombination processes given by:

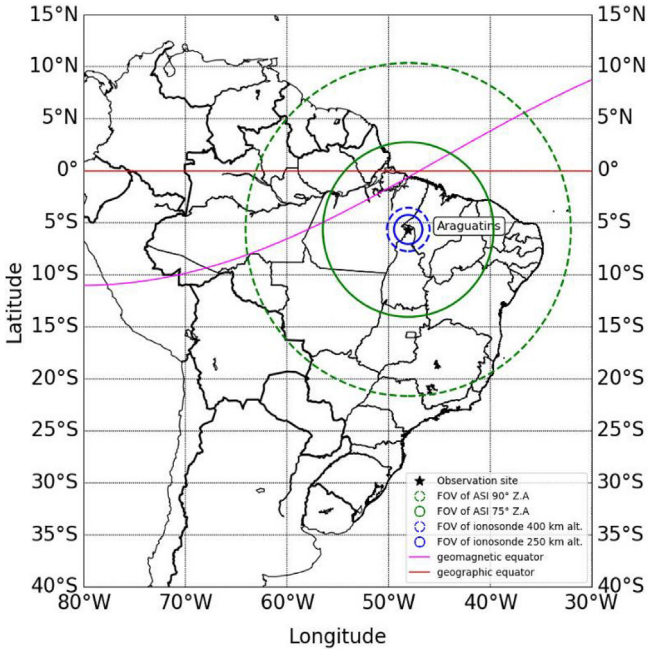

Fig. 1. A Brazilian map marking the Araguatins' observation site (5.65° S, 48.07° W and dip-latitude of 4.17° S) with a black star, the geographic equator with a red horizontal line, and the geomagnetic equator with a magenta curve. The FOV of the ASI at 75° (solid) and 90° (dashed) Z.A. and ionosonde at 250 km (solid) and 400 (dashed) km are shown as green and blue circles, respectively. (For interpretation of the references to colour in this figure legend, the reader is referred to the web version of this article.)

$$O_2^+ + e^- \rightarrow O + O^*(\ ^1D) \quad (1)$$

$$O^*(\ ^1D) \rightarrow O + h\nu(630nm) \quad (2)$$

where * is the excited state. In the F_2 region, the rate of reaction given in equation (1), is proportional to the rate of recombination in the layer. The OI630.0 nm emission intensity observed is proportional to the column integral of the product of O_2^+ (charge transfer) and e^- (electron density) concentrations in the F-region. The variation of the OI630.0 nm nightglow intensity in response to the variation

of the height of F-region electron density peak makes these kinds of measurements valuable for the study of height related ionospheric F-region phenomena.

The Canadian Advanced Digital Ionosonde (CADI) which operates at vertical incidence with transmission frequencies between 1 and 20 MHz was used simultaneously with the ASI system at the same observation site. The CADI ionosonde comprises a delta antenna transmitter, a four-dipole receiver, and a frequency synthesizer. The power requirement of the transmitter is ~ 600 W and provides the power amplification of radio frequency (RF) signals. The receiver consists of a standard wideband RF amplifier, a mixer, and a narrow intermediate-frequency amplifier. The receiver amplifies and demodulates the returning signals that bounced off of the ionosphere. The frequency synthesizer uses the direct digital synthesis card, which produces two output frequencies from its two channels. The CADI ionosonde covers an altitude range between ~ 90–1000 km with a ± 3 km resolution from a pulse length of 40 μs. The system operates in two scanning modes, with the first being 180 frequencies every 300 s for normal ionogram output. The second mode scans 6 frequencies (3, 4, 5, 6, 7, and 8 MHz) every 100 s in higher temporal resolution. For noise suppression, the CADI ionosonde uses a coherent pulse averaging to improve the signal-to-noise ratio. The CADI allows to get ionospheric parameters and to manually identify nighttime plasma density profiles and Spread-F configurations from the ionograms. The ionograms from the CADI are obtained at 5-minute intervals. This ionosonde operates routinely and probes the sky at the same time as the ASI. The presence or absence of equatorial range Spread-F are identified in the ionograms to compare with the occurrence of bubbles and/or blobs in the OI 630.0 nm nightglow images.

Three identical satellites called Swarm A(lpha), B(ravo) and C(harlie) make up the so-called Swarm constellation (Friis-Christensen et al., 2006, 2008; Pezzopane and Pignalberi, 2019). The three satellites were launched into circular near-polar orbits with 87.4° inclination at the end of 2013 by the European Space Agency with the main aim to study the Earth's magnetic field. The initial altitude of satellites was 500 km. Later, Swarm A and C, flying side-by-side (lower pair), changed their altitude to 470 km with 1.4° separation in longitude (approximately 6 min in local time). Swarm B, instead, increased its altitude to 520 km in an orbital plane which has gradually got farther away from those of the other two satellites during the mission's lifetime (9 h in local time after 4 years). Among the payloads installed onboard the satellites is the Langmuir probes for the measurement of plasma density. The results presented in this study were obtained by using Level 1b electron density measurements at 2 Hz rate (EFIx_LP) made by Langmuir probes. Specifically, values of electron density measurements recorded by the Swarm constellation at higher altitudes above the F-layer peak height will be considered to complement the results obtained from ASI system and the ionosonde.

The geographical location of the observation site (black star), ARA where the ionosonde and all-sky imager are operating is shown on the Brazilian map in Fig. 1. Also, on Fig. 1 are shown the geographic (red line) and the geomagnetic (magenta curve) equators. The green dashed and solid circles are the imager's field of view at 90° and 75° zenith angles, respectively at 250 km altitude. At 90° Z.A., the ASI covers ~ ± 16° lat/lon which corresponds to a diameter of ~ 3500 km. The latitudinal and longitudinal extent at 75° Z.A. is approximately ± 8° lat/lon with horizontal diameter of ~ 1800 km (Mendillo and Baumgardner, 1982). The blue dashed (solid) circle represents the FOV of the ionosonde at ~ 400 (~250) km, corresponding to a horizontal diameter of ~ 462 (~288) km which is approximately ± 2.1° (±1.4°) lat/lon (Alfonsi et al., 2013).

3. Data analysis

Sample nightglow and ionogram observations for the nights 07 March 2017, 29 September 2017 and 12 October 2017 are shown in Fig. 2 from top to bottom, respectively. During nighttime, it is possible to measure OI 630.0 nm nightglow emissions using All-Sky Imaging Systems. Sample images from the imaging system located at ARA are shown in Fig. 2 (left panel). Fig. 2 (right panel) present respectively ionograms for each of these different events. The Figure show OI 630.0 nm nightglow images with no plasma bubble/blob, only plasma bubble and plasma bubble-blob corresponding to ionograms showing F-layer echoes with no ESF, only typical ESF, and atypical ESF, respectively. Using these 3 examples from simultaneous and collocated ground-based observation it will be possible to establish a methodology to identify in ionograms the occurrence of plasma bubble or when there are occurrence of plasma bubbles and blobs simultaneously in the field of view of the ionosonde.

The first event (Fig. 2a) is when there are no irregularities or waves observed in the all-sky field of view and it is possible to notice that the OI 630 nm nightglow emission has its intensity almost homogeneous. The simultaneous ionogram recorded shows clearly the first F-layer reflection (hereafter FR1) with ordinary and extraordinary traces (echoes) as seen in Fig. 2a, right panel. In addition, it is also possible to see the second and third F-region reflections (here on after referred to as FR2 and FR3 respectively), as shown in the ionogram (Fig. 2a – right panel). Notice that all 3F-region trace echoes are quite similar in shape or configuration and comparable in their critical frequencies.

In the second event, OI 630.0 nm nightglow emission image only shows depletions - dark, north–south structures almost aligned to the Earth's magnetic field (Fig. 2b – left panel); this is the signature of large-scale ionospheric irregularities (Plasma bubbles). The simultaneous ionogram show typical signature of range Spread-F (Pillat, Fagundes, and Guimarães, 2015) whose echoes go up to

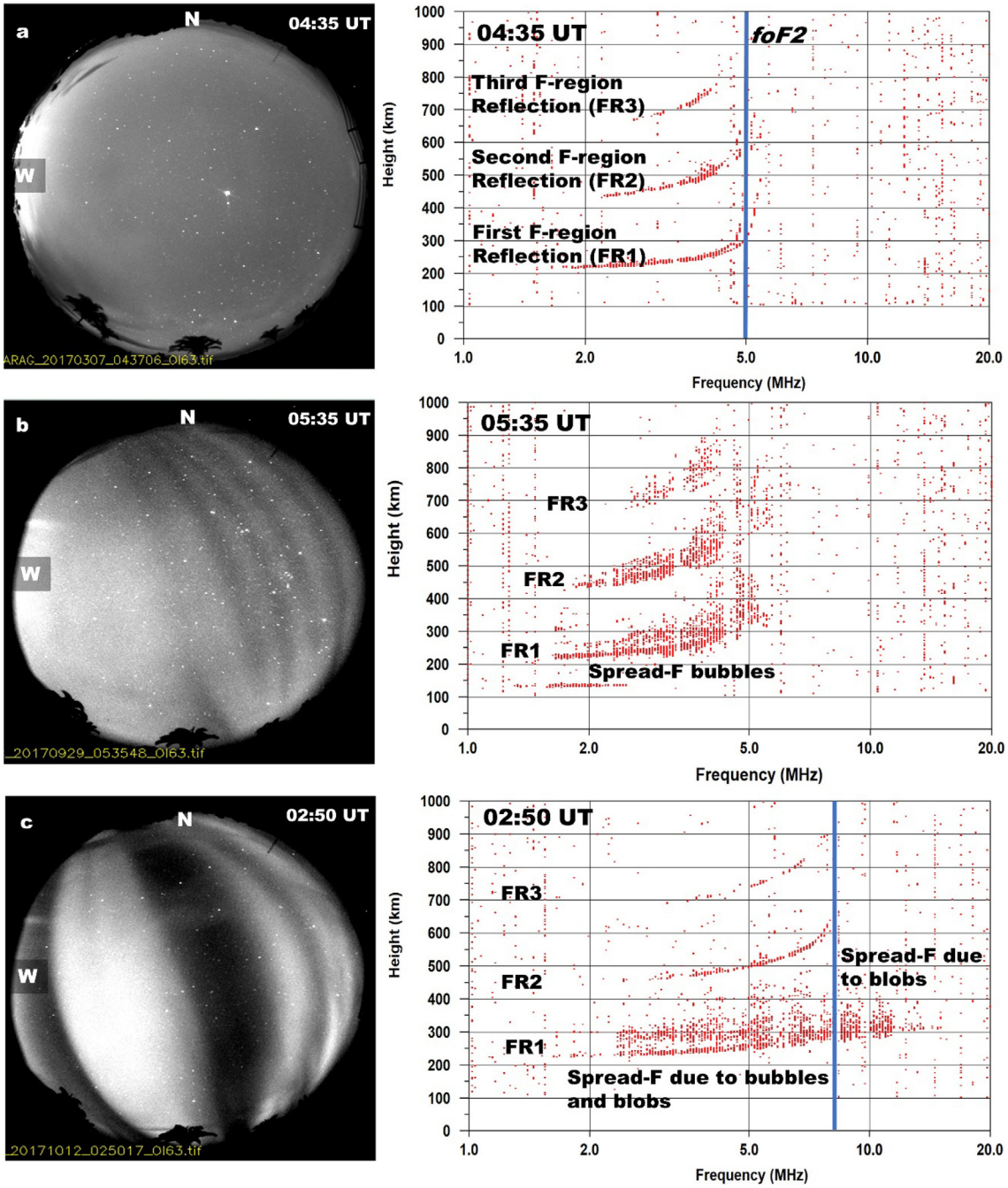

Fig. 2. Shows sample of OI 630.0 nm nightglow emission observations and ionograms for 3 different cases. a) 07 March 2017 with no plasma bubble or waves, b) 29 September 2017 showing plasma bubbles (dark bands) and range Spread-F and c) 12 October 2017 show bubbles (dark bands) and blobs (bright bands) with atypical range Spread-F ionograms. Ionograms for all the events show the first, second and third F-region reflection echoes.

a frequency of 5 MHz (Fig. 2b – right panel). Notice that the first, second and third F-layer reflection echoes recorded have quite similar shapes.

The third case is when the OI 630.0 nm nightglow image show dark and bright north–south bands almost aligned to the Earth geomagnetic field (Fig. 2c-left panel), these structures are identified as bubbles and blobs, respectively. We see the blobs extending across the image from the north to the south of the observation site toward the EIA crest region. This could probably be an extension of the southern anomaly crest in the field of view of the imaging system. The blobs shown have homogeneous longitudinal intensity and are almost aligned to the magnetic field (following nearly the same latitudinal shape as the plasma bubbles). Fig. 2c (right panel) shows the ionogram recorded at almost the same time as the nightglow OI 630.0 nm emission image, and it is possible to notice that the echoes present an atypical kind of range Spread-F. First, the range Spread-F frequencies go up to and beyond 10 MHz and the first F-region trace echoes are quite different from the

second or even third F-region reflection echoes in terms of configuration (shape) where the part associated with high plasma density reflections (blob) does not appear in the second and third reflections. Indicating that this ionogram recorded have superimposed the signature of the bubble and blobs as well. This assumption is only possible because we have simultaneous observations of OI 6300 nm nightglow emissions and ionogram. The blue vertical lines in Fig. 2c indicate the echoes at higher frequencies from high plasma density regions. This ''threshold'' frequency can be inferred from the second reflection of the F-layer if it exists as shown below or it can be obtained from ionograms on the same night when no irregularities were present. An ESF structure is considered ''atypical'' when high-frequency echoes from blobs - after blue vertical line, and low-frequency echoes from plasma bubbles (''typical'' ESF) - before blue vertical line, occur together.

To show the association between the observed structures in the nightglow images and the ionograms, nightglow images showing different structures have been selected as case studies in this paper. The ionograms recorded simultaneously with these nightglow images were also selected to identify the range Spread-F structures. UASDA - a software developed at UNIVAP nightglow image studies, was used to analyses and study the OI 630.0 nm nightglow images of the structures observed in the events under study. The ''scanning method'', first introduced and described by Pimenta et al. (2001), was employed to determine the emission intensity along a scanning line passing across the nightglow images and structures from west to east after the images have been linearized (see sample results in Fig. 3). This way plasma density enhancements and depletions can be estimated. Sample analyses for selected pair of images have been shown for each Figure in the preceding section.

Fig. 3 (left panel) shows linearized OI 630.0 nm nightglow images with: a) background ionosphere, b) plasma bubbles and c) plasma blobs (and bubbles). The white stars on the images show the observation site and the blue circle shows the field of view of the ionosonde at 400 km altitude over the observation site. In Fig. 3a, the green, vertical line in the intensity plot denoted as star, is the intensity of light emission from a star which has a much higher intensity compared to the OI 630.0 nm night glow emission intensity. In Fig. 3b and c, it is worth noting that plasma bubbles and blobs fall inside the FOV of the ionosonde making it possible for the ASI and ionosonde to observe simultaneously ionospheric irregularities that pass over the observation site. In the right panel, we show the relative nightglow intensity variation obtained from the OI 630.0 nm nightglow images for different cases in arbitrary units.

The red and green horizontal lines on the pair of OI 630.0 nm nightglow images (in a, b and c) represent the path along which the relative emission intensities were determined at different times and they correspond to the red and green curves in the intensity plots in the right panels. The dashed black horizontal lines show the background relative OI 630.0 nm nightglow intensities where the intensities are uniform and do not show great depressions or enhancements (See Fig. 3a right-panel). Since the plasma density and consequently airglow intensity varies greatly day-to-day and throughout the night, the plots presented show different values (horizontal dashed lines) for the background relative intensity that helps to distinguish between high and low relative intensity at any point in time for blobs and bubbles, respectively. By plotting the relative OI 630 nm nightglow intensities from the recorded images using the pixel values and considering all the known properties of a bubbles and blobs, we are able to determine where we have high intensities (increased plasma density) corresponding to blobs and low intensities (reduced plasma density) corresponding to bubbles. When structures in the images are compared with the profile in the plots, it can be seen that the high and low intensity structures in the profiles occur in the same longitudes as the bright and dark bands in the OI 630.0 nm nightglow images that depict them. Fig. 3a left panel shows the intensity plot when there is no increased or decreased plasma density producing a uniform relative OI 630 nm nightglow intensity plot. Here it is easy to note from the profile that there are no bubbles or blobs. Plasma blobs (bubbles) are the localized enhancements (depletions) in the OI 630.0 nm nightglow relative intensities with respect to the background (Webber et al., 1978; Mendillo and Baumgardner, 1982; Nade et al., 2014; Sharma et al., 2018) as demonstrated here in the figures.

Using this method, the plasma blobs presented here were determined to have emission relative intensities from ~ 40% to ~ 80% above the ambient emission intensity for all the cases presented. The percentage increase in nightglow intensity corresponds to enhancement in plasma density in that region. The increase in plasma density is defined relative to the background ionospheric plasma density in that region at the time of observation. Since there is no threshold of plasma density for the identification of plasma blobs, different researchers have used different enhancement values as has been done in this work.

4. Observations and results

In this section, nightglow images, ionograms and electron density plots from Swarm satellite measurements are shown and compared for each study case. We divided the cases into three; 1) absence of plasma structures (bubbles/blobs) or waves– one case, 2) presence of plasma bubbles – one case and 3) occurrence of plasma blobs (with bubbles) – six cases. For each case, nightglow images and corresponding ionograms, showing the different echo features associated with the irregularities are presented. The three groups were compared to determine the presence or absence of irregularity structures. Each ASI image, ionogram and Swarm plot are shown in universal time (UT) (for ARA LT = UT – 3 h).

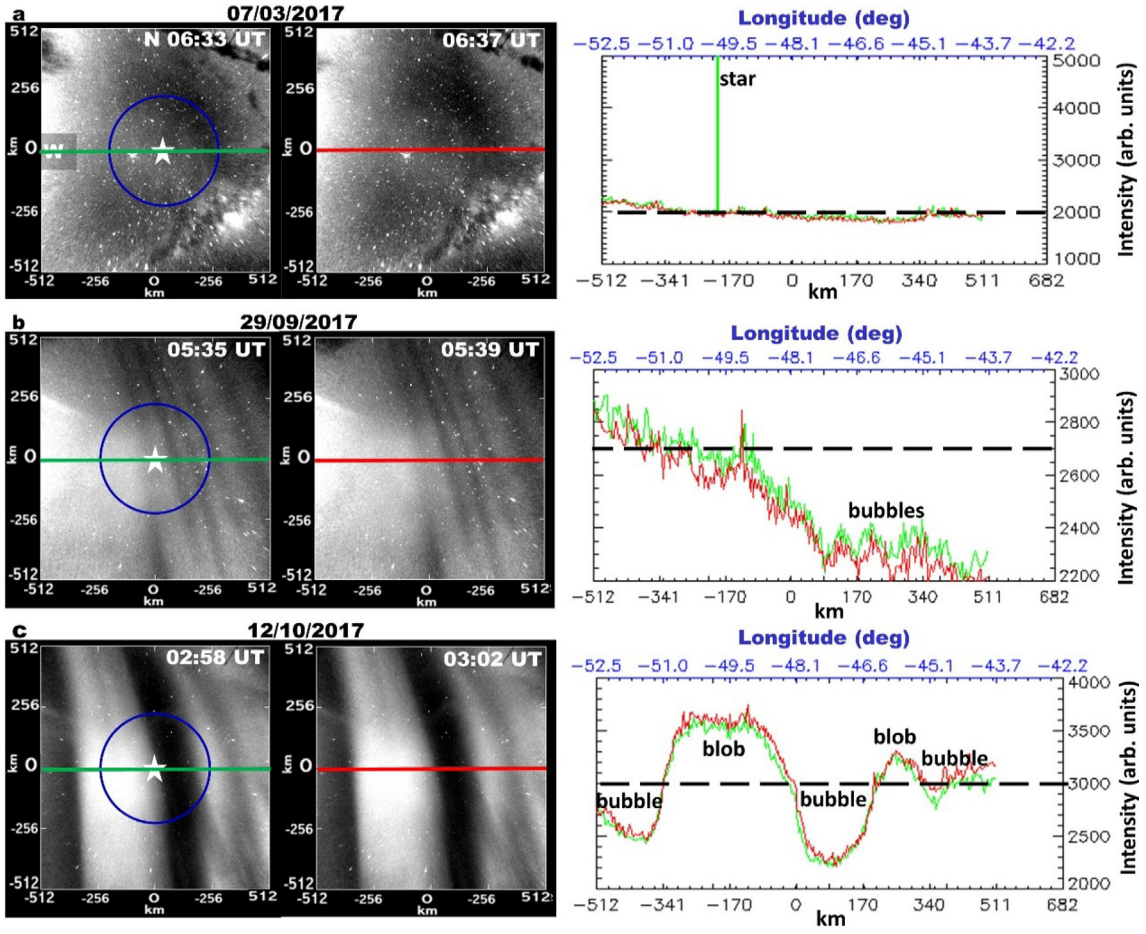

Fig. 3. a) linearized OI 630.0 nm nightglow image for March 07, 2017 at 06:33 and 06:37, the star is the observatory location on the image, blue circle is the ionosonde FOV, and green and red lines indicate the scanning path across the OI 630.0 nm nightglow images (left panel). OI 630.0 nm nightglow relativity intensity plots along the scanning paths. Bubbles or blobs are indicated when they occur (right panel). b) The same as a) but for September 29, 2017. c) The same as a) but for October 12, 2017. (For interpretation of the references to colour in this figure legend, the reader is referred to the web version of this article.)

4.1. Absence of irregularities (07 March 2017)

Fig. 4a shows a sequence of OI 630.0 nm nightglow emission images obtained over ARA station in Brazil. The OI 630.0 nm images shown have a time resolution of around 20–30 min. The sequence of images shows no signs of ionospheric irregularities (depletions/enhancements) or even waves. The homogeneity observed in the OI 630.0 nm nightglow images is indicative of the absence of structure in the ionosphere inside the field of view of the ASI. Fig. 4b show sample linearized OI 630.0 nm nightglow images used to determine the relative emission intensity of the OI 630.0 nm emission for the same night. The relative OI 630 nm nightglow intensity plot shows an almost linear plots of the relative intensity with no enhanced (high intensity) or depleted (low intensity) regions or even wave-like structures in the ionosphere. This is typical of background OI 630.0 nm emission intensity profile as seen in the raw nightglow in Fig. 4a. It is worth noting that the OI 630 nm emission intensity profile presented here is representative for the period only between ~ 04:30 UT and ~ 06:30 UT and not for the entire night as airglow intensities vary greatly throughout the night.

In the absence of irregularities or waves in the OI 630.0 nm images, the ionograms recorded simultaneously shows a clear nighttime F-layer bottom side profile with the ordinary and extraordinary traces in Fig. 4c. The ionograms also show the First and Second F-region reflections of the F-region ionospheric profile. All the F-region traces observed in the ionograms look similar in form. During this period, the background critical frequency (*fo*F2) recorded in the ionograms was less than 5 MHz.

Fig. 4d shows the plots for plasma density measurements from the Swarm constellation. The Swarm satellites make plasma density measurement in the ionosphere above the F-layer peak heights. In the left panel, the figure shows the FOV of the ASI (green circle) at 250 km altitude corresponding to Z.A. of 75° and horizontal radius of ~ 933 km. In the left panels are shown the flight paths of the satellites and in the right panels are shown the geographic latitudinal electron density variation graphs.

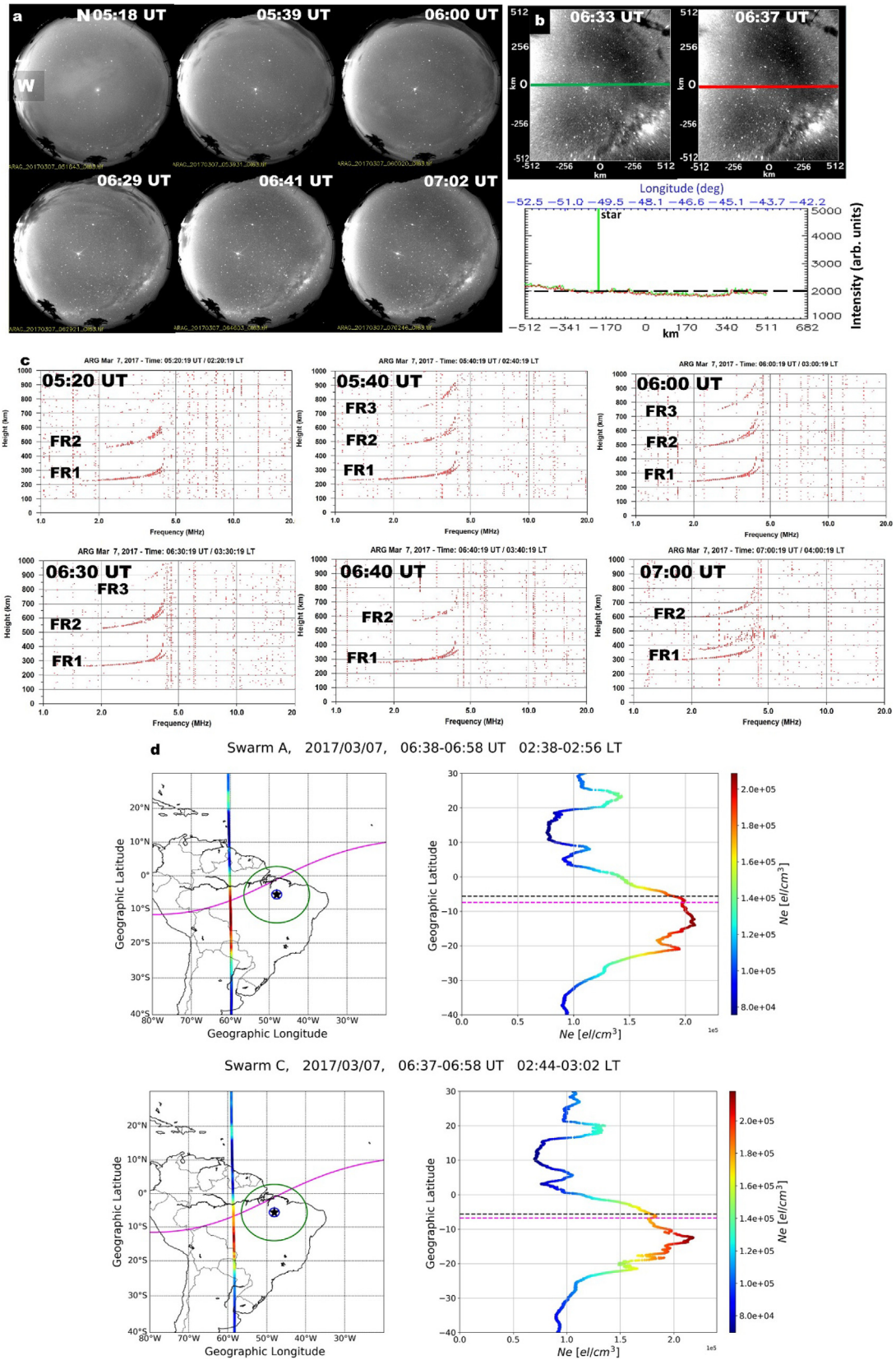

Fig. 4. Multi-instrument observations on the night of 07 March 2017 between 04 and 07 UT. a) Nightglow images, b) Linearized nightglow image pair with nightglow intensity plot, c) ionograms, d) Electron density measurements from Swarm A and C (the magenta line is the geomagnetic equator, green and blue circles represent FOV of ASI and ionosonde, respectively. The black star on the left as well as the horizontal black dashed line on the right panel mark the location of ARA). (For interpretation of the references to colour in this figure legend, the reader is referred to the web version of this article.)

Above the F-layer peak heights, over the Brazilian ionosphere, Swarm A and C observations show plasma density measurements with high plasma density near the geomagnetic equatorial and some wavelike oscillations at low latitudes regions. The plasma density measurements for both Swarm A and C were conducted between 02:38 LT and 03:02 LT. Therefore, the typical signature of plasma bubbles or blobs with high density fluctuations are not observed. The ground based (OI 630.0 nm nightglow and ionosonde) and in situ observations agree. Note that the path of the Satellites falls outside of the fields of view of both the all-sky imager and the ionosonde, as such any discrepancy in the observation results could be because of it.

4.2. Observation of only plasma bubbles (29 September 2017)

In this section the OI 630.0 nm emission nightglow presented in Fig. 5a show several north–south, dark bands of depleted plasma density on bright OI 630.0 nm emission background. The dark bands are almost aligned along the Earth's geomagnetic field lines. These are the signatures of nighttime ionospheric plasma bubbles. In contrast with the results in Fig. 4a, the OI 630.0 nm nightglow emission images in Fig. 5a are not homogenous but show depleted band (bubbles) across the images. The bubbles drift eastward in the field of view of the imager system. Note that the brightness on the left side of Fig. 5a is not as a result of blob but possibly light from an external source. This is because this light source does not move with the bubble as the bubbles drift eastward from the west compared to all the cases of blobs presented in the manuscript. The brightness stays in the same location even with the passing of time. The OI 630.0 nm relative intensity plots from the linearized nightglow images in Fig. 5b (upper panel) show relative intensities below the nighttime background emission intensity. There is a clear nightglow intensity reduction in the lower panel of Fig. 5b which resulted from plasma depletions (plasma bubbles). The result is different from Fig. 4b which does not show such depressions in the OI 630.0 nm emission intensity due to the absence of plasma bubbles or waves.

Meanwhile, the simultaneous ionograms in Fig. 5c show typical signatures of range equatorial Spread-F. Since Spread-Fs are known to be irregularities of different scale sizes found inside plasma bubbles observed in ionograms they present evidence of plasma bubbles in ionosonde observations. Therefore, the ESF observed in the ionograms in Fig. 5c show the occurrence of depleted plasma irregularities, also plasma bubbles. Since ESFs are normally associated with depleted plasma regions, the echoes are expected to have frequencies below the normal nighttime critical frequency. The ionograms presented here show ESF echoes are observed up to frequencies of ~ 5 MHz on this night which means that the plasma density is reduced within these regions. The ionograms also show the second and third F-region reflections. For reference, the first, second and third F-layer traces have similar shapes or configurations.

During this period only the Swarm B satellite passed within the field of view of the both the ionosonde and the imager system. The observation took place after midnight hours local time. The latitudinal plasma density measurement is in Fig. 5d. The plot shows along the path of the satellite strong plasma density fluctuations inside plasma depleted regions which is the signature of the large-scale ionospheric irregularities observed as dark bands in the OI 630.0 nm images and as range Spread-F in the ionograms from the ionosonde. The plasma density plots also show high plasma density peak in the southern hemisphere which was not observed by either the ASI or ionosonde. The disparity could be due to the fact that the Swarm satellite takes measurement from the topside ionosphere while the ground-based observations are made at the bottomside of the ionosphere and as ESF is associated with irregularities at the bottom side, the plasma density peak observed might be only at higher altitudes above the bottom side. It could also be due to the small-time difference between the satellite passing and the commencement of the ground-based measurements shown below.

4.3. Observation of bubbles and blobs

4.3.1. Occurrence of blob and bubbles (14 September 2017)

The OI 630.0 nm emission night glow images and ionograms in this section show representative results for the observation of plasma bubbles and blobs and their association with atypical range Spread-F features observed simultaneously in ionograms recorded almost the same time as the OI 630.0 nm nightglow images.

Fig. 6a shows the occurrence of dark and bright structures which are aligned north southward to the Earth's magnetic field. These structures are plasma bubbles and blobs, respectively. The blob, though looks rounded at the center, seem to show a trail originating from southward of the image extending from the EIA crest region. This could mean that the EIA could possibly move plasma into the equatorial region during to sunset hours and thereby influencing the occurrence of plasma blobs as shown in the OI 630.0 nm nightglow images. The plasma blob is seen to be oriented along the magnetic field of the Earth as the plasma bubble. At 01:43 UT 02:04 UT, the bubble is large and almost covers the entire surface of the image, but traces of the blob can be seen to appear at the west edge of the images. The blob later on becomes much visible and brighter at the center of the image between 02:25 UT and 03:27 UT. Fig. 6b clearly shows in the relative nightglow intensity plots regions of increased and decreased emission densities corresponding to plasma blob (blue arrow) and bubble (green arrow), respectively.

Fig. 6c shows atypical range Spread-F structures associated with the plasma bubbles and blobs seen in the OI 630.0 nm nightglow images. The ionograms show range

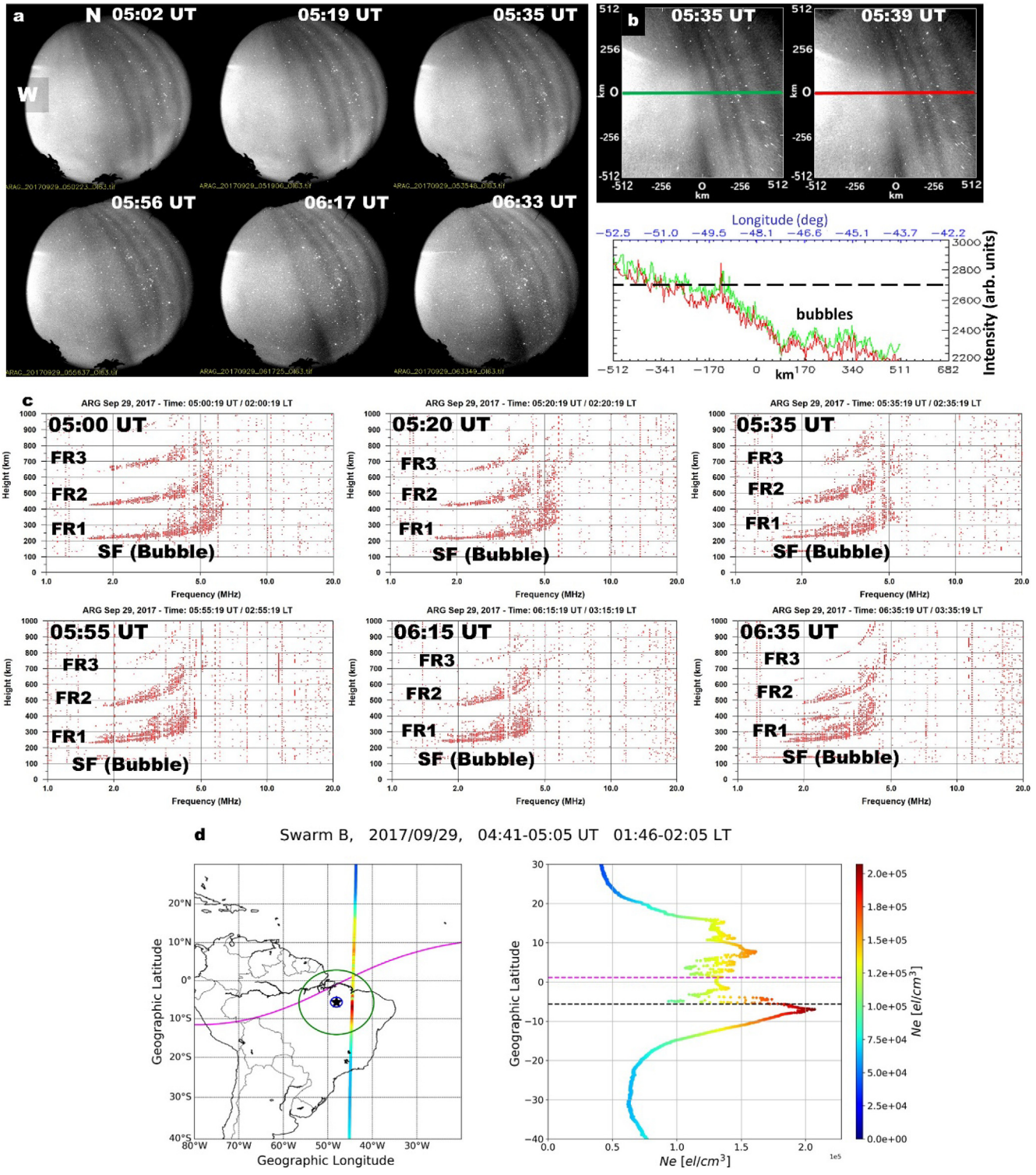

Fig. 5. Same as Fig. 4 but for the night 29 September 2017 showing the occurrence of only plasma bubbles.

spread-F associated with bubbles and blobs (low-frequency echoes) and blobs (high-frequency echoes) separated by the vertical blue line. As the square of the frequency is proportional to the plasma density of the F_2 peak layer the echoes on the ionograms correspond to plasma density as plasma depleted regions will reflect signals at lower frequencies while plasma enhanced regions will reflect signals at higher frequencies. In all the ionograms seen in Fig. 6c, the range spread-F echoes are seen at higher frequencies of up to and beyond ~ 10 MHz signifying the occurrence of plasma blobs.

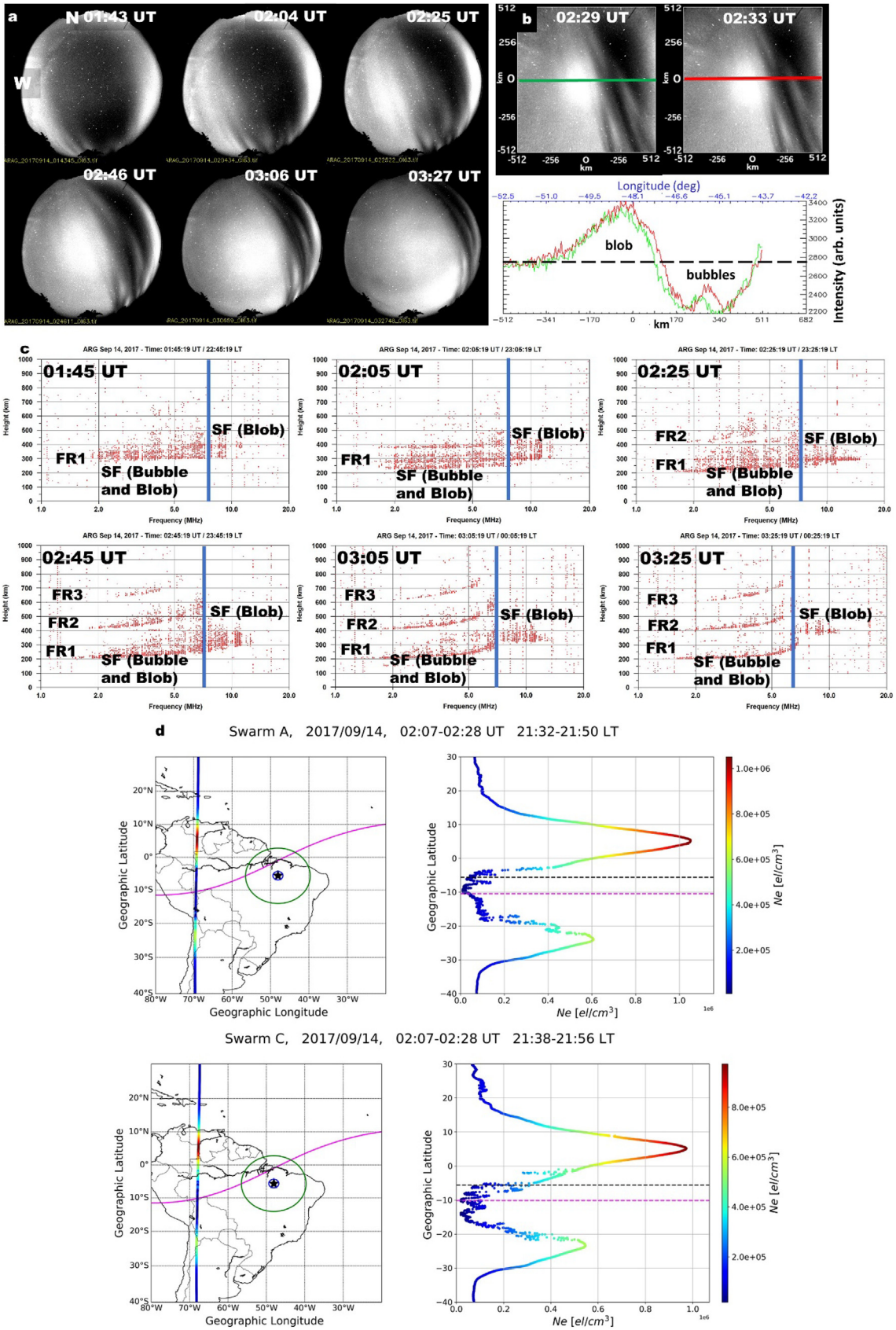

Fig. 6. Same as Fig. 5 but for the night 14 September 2017. a) nightglow images with plasma bubbles and blobs, b) linearized nightglow image pair and nightglow intensity plot, c) ionograms showing atypical ESF d) electron density measurements from Swarm A and C.

F-region reflections do not occur until about 02:25 UT when the ionograms begin to show reflections of the ionospheric F-layer. We begin to see the second and third F-region reflections (FR2 and FR3 respectively) clearly from between 02:45 UT to 03:25 UT. The reflections observed, when plasma blobs are present in the company of plasma bubbles in the OI 630.0 nm nightglow, unlike when there no irregularities or there is only the occurrence of plasma bubbles are different as seen in Fig. 6c. We see that the reflections occur up to where the high-frequency echoes associated with the plasma blobs occur.

Electron density measurements showing plasma density variations are shown in the plots of Fig. 6d. From Fig. 6d, the paths of the satellites are far away from the fields of view of both the imaging system and the ionosonde as shown. At the Swarm heights, around 02:00 UT over Brazil, it is possible to observe remnants of the EIA crests and trough. The signatures of the EIA could not be observed in the relative plasma density plots in Fig. 6b due how far the satellites paths were from the FOVs of the ground-based observations, however, the EIA observed by the Swarm satellites might have had influence on the plasma blobs observed in the OI 630.0 nm nightglow images. It can also be seen that in the crests of the of the EIA, there are no plasma density fluctuations, but smooth rounded peaks. On the other hand, in the trough, around the observation latitude, strong plasma density fluctuations are seen. These plasma density fluctuations could be signatures of the equatorial plasma bubbles. The results from the in-situ observation are consistent with the ground-based remote sensing observations.

4.3.2. Occurrence of blob and bubbles (12 October 2017)

Fig. 7a shows OI 630.0 nm nightglow images with dark and bright north–south aligned bands of plasma bubbles and blobs. The nightglow images show bubbles and blobs between on:47 UT and 3:31 UT on 12 October 2017. The blobs just like the bubbles are inclined along the geomagnetic field lines of the Earth. Sobral et al. (2011), studying the westward plasma bubble drift, stated the importance of bubbles being aligned to the geomagnetic field lines as it allows to study their zonal motion, which is necessary to understanding ionospheric dynamics. Also, plasma density inside the blob is homogenous in nature longitudinally with shape and alignment almost like the plasma bubble. It can be seen that the blobs are extending to or originating from the south of the observation site toward the EIA crest region. This could probably be an extension of the southern anomaly crest in the field of view of the imaging system with the EIA crest influencing the plasma density in the region. The relative OI 630.0 nm nightglow emission intensity plots in Fig. 7b shows regions of enhanced and depleted emission intensities representative of a blob and a bubble, respectively.

The ionograms recorded simultaneously as the OI 630.0 nm nightglow images show range Spread-F structures shown in Fig. 7c. The echoes show an atypical ESF structure with low- and high-frequency echoes going up to and above ~ 10 MHz at different times. In the ionograms of the lower panel of Fig. 7c, we observe multiple F-region reflections (FR2 and FR3). This event also shows that the reflections in the ionograms, when they occur in the presence of a blob, present structures that are different from the FR1 trace. The FR2 and FR3 reflections always show the part of FR1 reflection echoes up to the blue vertical line but not the higher frequency echoes associated with the plasma blobs similar to the results section 4.3.1.

Fig. 7d shows the plasma density variations plots from Swarm B measurements carried out after midnight hours local time over Brazil. Inside the field of view of the ground-based instruments are observed several structures of plasma density maxima and minima, with density fluctuations, which are the signatures of plasma blobs and bubbles, respectively. In either of the hemispheres (north and south), we observe crests of plasma density which could be the EIA. The two EIA crests are seen outside of the field of view of the ground-based instruments as can be seen in Fig. 7d. This means that the plasma density enhancement observed by the ASI and the ionosonde could not be the plasma density enhancements in the crests of EIA but plasma bubbles. On the hand, even though the EIA crests could not be observed directly from the ASI and the ionosonde due to their relative positions, the EIA could be considered as providing the background plasma density for the observed plasma blobs. Also, the path of the satellite is inclined to the plasma blobs tilted along the geomagnetic field lines, as such the Swarm satellites passes over and cutting through regions of high plasma density, then low plasma density and again high plasma density showing peaks and trough we observe in the Swarm plots. Inside the plasma density minima and maxima, we observe plasma density fluctuations which shows that there are irregularities inside the depleted and enhanced regions which shows why the atypical structures have range spreads even at higher frequencies. The results from the ground-based observations at the base of the ionosphere agree with the satellite results.

4.3.3. Occurrence of blob and bubbles (21 October 2017)

This event presents another case of plasma depleted and enhanced structures, dark and bright regions respectively in the OI 630.0 nm nightglow images in Fig. 8a. The structures have the signatures of bubbles and blobs. They are inclined along the magnetic field lines; they have latitudinal extensions and are north–south oriented. The blobs extend north–south covering various latitudes with the brightest region in the center and fading towards the north and south edges of the images in the direction of the anomaly crest regions. As such we could infer that the plasma blobs observed could have been at least partly as a result of the south EIA crest shifting towards the observation region under the influence of thermospheric winds. The OI 630.0 nm nightglow emission relative intensity plots in

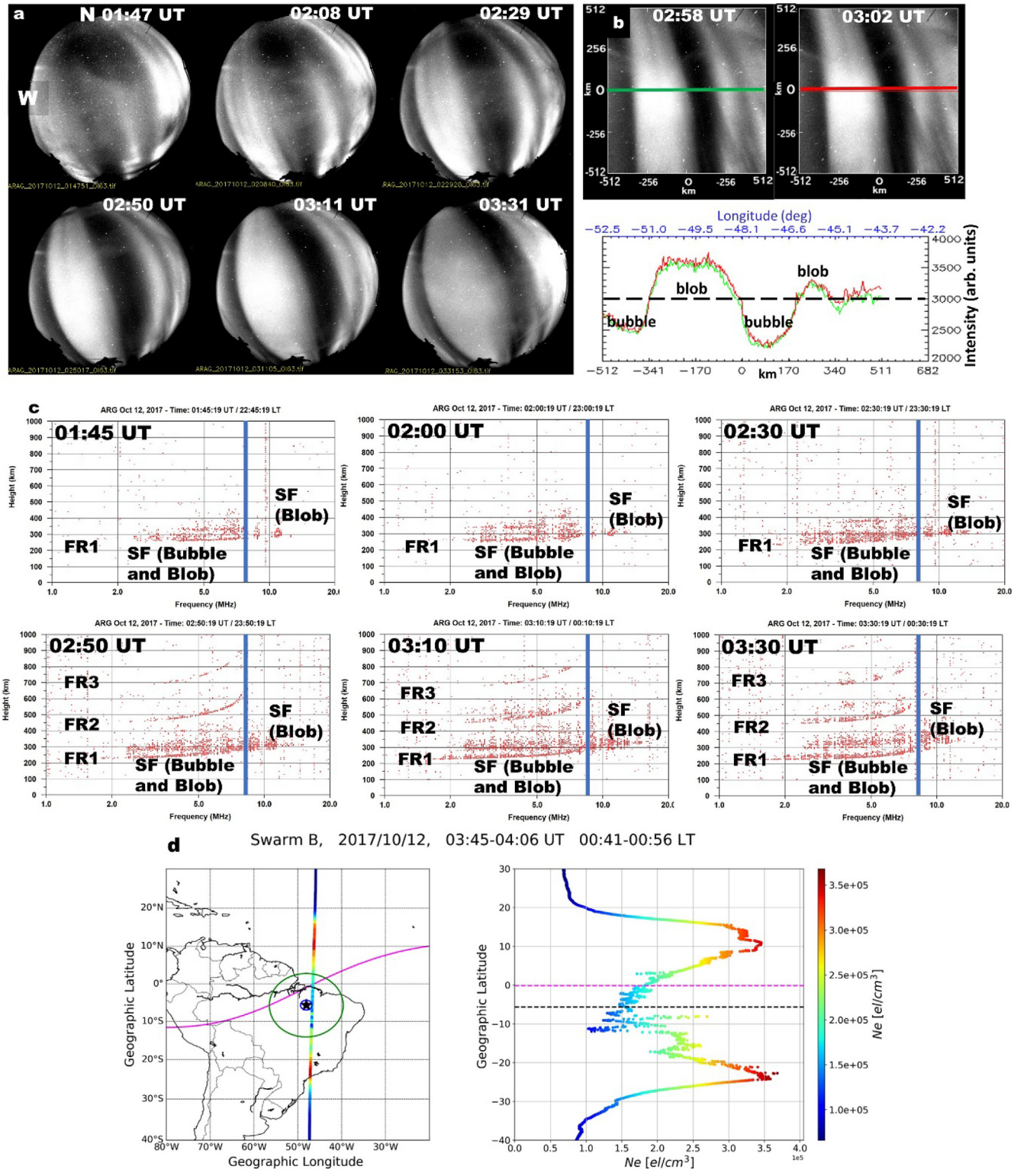

Fig. 7. Same as Fig. 6 but for the night 12 October 2017. Plasma density measurements are those from Swarm B.

Fig. 8b shows, significant increase in intensity above the background indicating that the observed bright regions in the raw nightglow images are indeed plasma blobs.

Fig. 8c shows the ionograms recorded in almost the same time as the OI 630.0 nm nightglow images. The ionograms show the occurrence of atypical ESF associated with the observation of plasma bubbles and blobs in the OI 630.0 nm nightglow emission images. The echoes go up to about ~ 15 MHz which signify the presence of localized high-density regions in the field of view of the ionogram

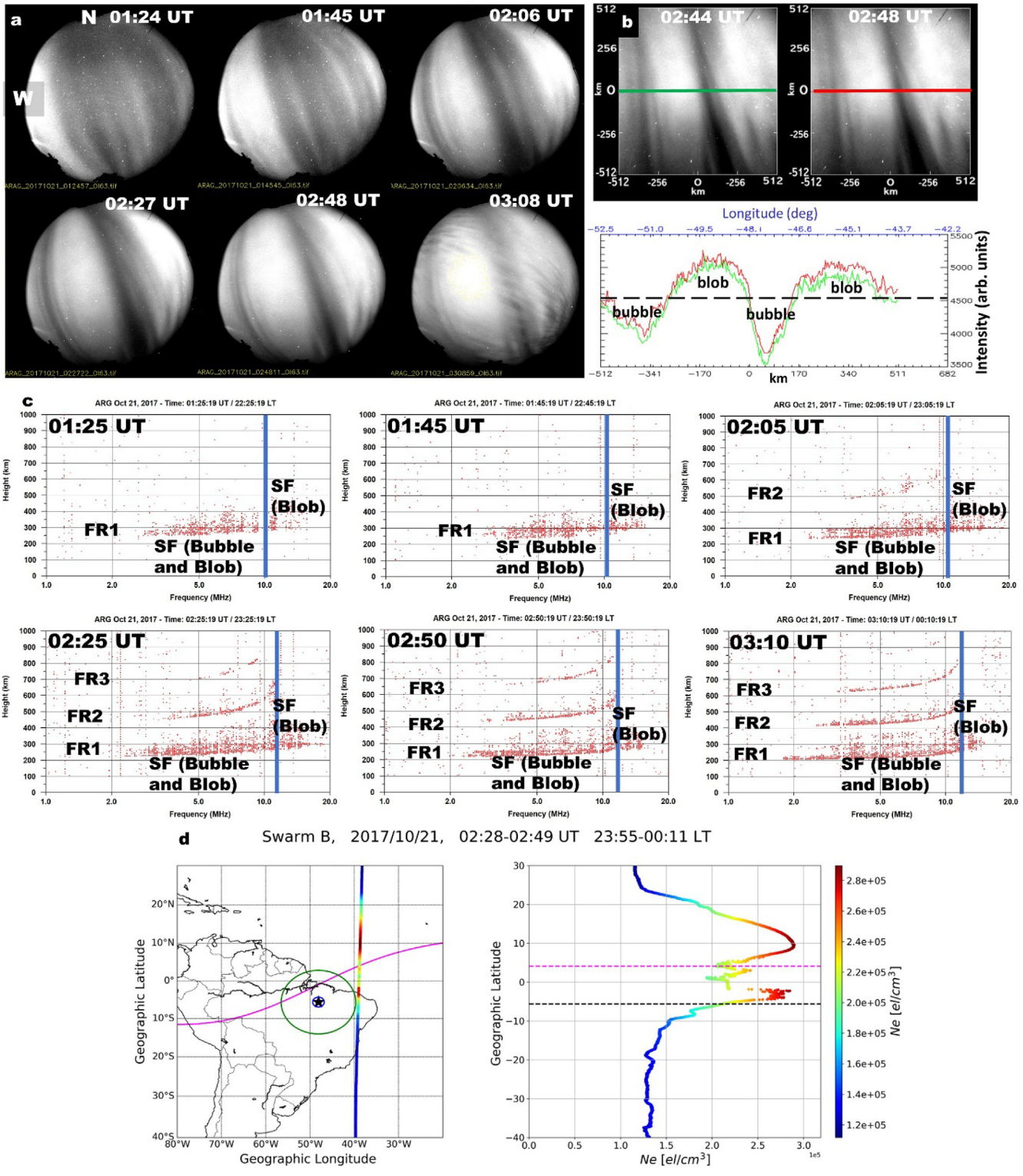

Fig. 8. Same as Fig. 6 but for the night 21 October 2017. Swarm measurements are those from Swarm B.

confirming the observation of blobs in the nightglow images. The FR2 and FR3 seen in the ionograms from 02:05 UT are different from the FR1 with the high-frequency echoes not showing in the higher order reflections indicating the superimposition of bubbles and blobs or at least the occurrence of blobs.

In Fig. 8d, plasma density measurements by Swarm B, shows a calm region of plasma density maxima peaking at 10° geographic north and other maxima at about 2.2° S. The satellite passes directly at the edge of the field of view of the ground-based instruments observing similar structures as in the airglow images. We see the EIA crests

from the electron density plots with the northern maximum shown a rounded peak with no fluctuations while the southern maximum shows several substructures and fluctuations inside the density peak. The southern maximum is seen right near the observations site. The EIA could have shifted, with the southern peak moving towards the equatorial region due to meridional winds. This could have moved plasma into the region to enhance the plasma density in the region, hence the observation of plasma blobs in the OI 630.0 nm nightglow images and atypical ESF in the ionograms could have been influenced by the shifting EIA structure. Between the two plasma density enhancements, at ~ 5° N, we see plasma density depleted region, below the background, associated with plasma bubbles. The results from the in-situ and ground-based observations agree.

4.3.4. Occurrence of blob and bubbles (23 October 2017)

The OI 630.0 nm nightglow images in Fig. 9a shows the simultaneous occurrence of plasma bubbles and blobs. Relative OI 630.0 nm emission intensity plot shows high and low intensity regions with respect to the background (Fig. 9b). In the ionograms, atypical range Spread-F echoes can be observed in Fig. 9c. Also, we can see that the FR2 and FR3, that begin to occur from 02:15 UT, show marked difference from the FR1 trace echoes. The ESF echoes show frequencies above 10 MHz, greater that the background critical frequency of less than 10 MHz (inferred from the FR2 and FR3).

Fig. 9d shows the plasma density measurements by the Swarm B on 23 October 2017. The plot highlights a significant plasma fluctuation along the path of the satellite which passes directly at the western edge of the FOV of the imaging system. The plasma density enhancements occur at ~ 4.5° N and ~ 12° S different from the locations of the daytime anomaly structure, however, it is known that the location the structure of the EIA is influenced by meridional winds which could account for the observed location of the plasma density peaks which could be the crests of the EIA. The EIA peaks seen in Fig. 9d can be seen to barely fall outside the FOV of the ground-based instruments, however, it could be said that the observed plasma blobs in the nightglow images could be directly or indirectly influenced by the variation of the ionization anomaly structure. Inside the high plasma density regions, we see strong fluctuations inside the regions. Plasma density minima with substructures associated with bubbles occur between ~ 5° and ~ 15° S.

4.3.5. Occurrence of blob and bubbles (20 November 2017)

Fig. 10a shows the simultaneous occurrence of plasma bubbles and blobs in OI 630.0 nm nightglow emission images. The bubbles and blobs extend from the north to the south and are inclined along the magnetic field lines of the Earth. Using the "scanning method", two successive images were linearized, and the relative OI 630.0 nm nightglow intensity plots were obtained showing the occurrence of high and low intensity regions inside the imager field of view (see Fig. 10b).

Fig. 10c shows ionograms recorded simultaneously as the OI 630.0 nm nightglow images. Like earlier events, the ionograms show the occurrence of atypical ESF as a result of the plasma blob observed in the company of plasma bubbles. Range Spread-F echoes are seen up to and above 10 MHz. Second and third F-layer reflections are seen only from 03:00 UT.

The plasma density plots in Fig. 10d from Swarm B shows a strong plasma density fluctuation inside the field of view of the ground-based instruments with several peaks and depletions associated with plasma blobs and bubbles, respectively. These density enhancements and depletions inside the region agree with the observations in the OI 630.0 nm nightglow images and the range Spread-F in the ionograms captured over ARA along the path of the satellite. The highest peaks (crests) in this graph occur around the equator inside the FOV of the ground-based instruments. Around ± 10°, we see remnants of the daytime EIA crests. The EIA peak observed at this time may have contributed to the formation of the blobs observed by the imager system and the ionosonde.

4.3.6. Occurrence of blob and bubbles (21 December 2017)

Fig. 11a show the occurrence of plasma bubbles and blobs in OI 630.0 nm nightglow images. The images show several bright and dark bands. These blobs and bubbles are north–south and are inclined along the geomagnetic field lines. Relative OI 630.0 nm intensity plot in Fig. 11b show several high intensity peaks relative to the background from left to right showing sequentially the bubbles and blobs.

The ionograms recorded at nearly the same time also show atypical ESF associated with the plasma bubble and blobs observed in the OI 630.0 nm nightglow images (Fig. 11c). The echoes in this event does not get up 10 MHz, however, we can see that the second and third F-layer reflections seen are different from the first F-layer reflection. They show similar behavior as the previous events with the FR2 and FR3 showing reflections for echoes of up to the blue vertical line. The reflections show different trace structures. They do not show the higher frequency echoes associated with the blobs.

At the edge of the field of view of the ground-based instruments, Fig. 11d shows plasma density measured by the Swarm satellites A and C after midnight hours. The plots from both measurements show plasma enhancements of various degrees at various locations with density fluctuations at localized regions. The plots show depleted regions with fluctuations as well. For Swarm A, the density variations showed peaks related to the plasma blobs with the EIA crests as the background, as seen in the nightglow images and ionograms. These density enhancements are between ~ 15° geographic north off the anomaly crest region and ~ 7° geographic south. For Swarm C, we see three high density plasma peaks at different latitudes than

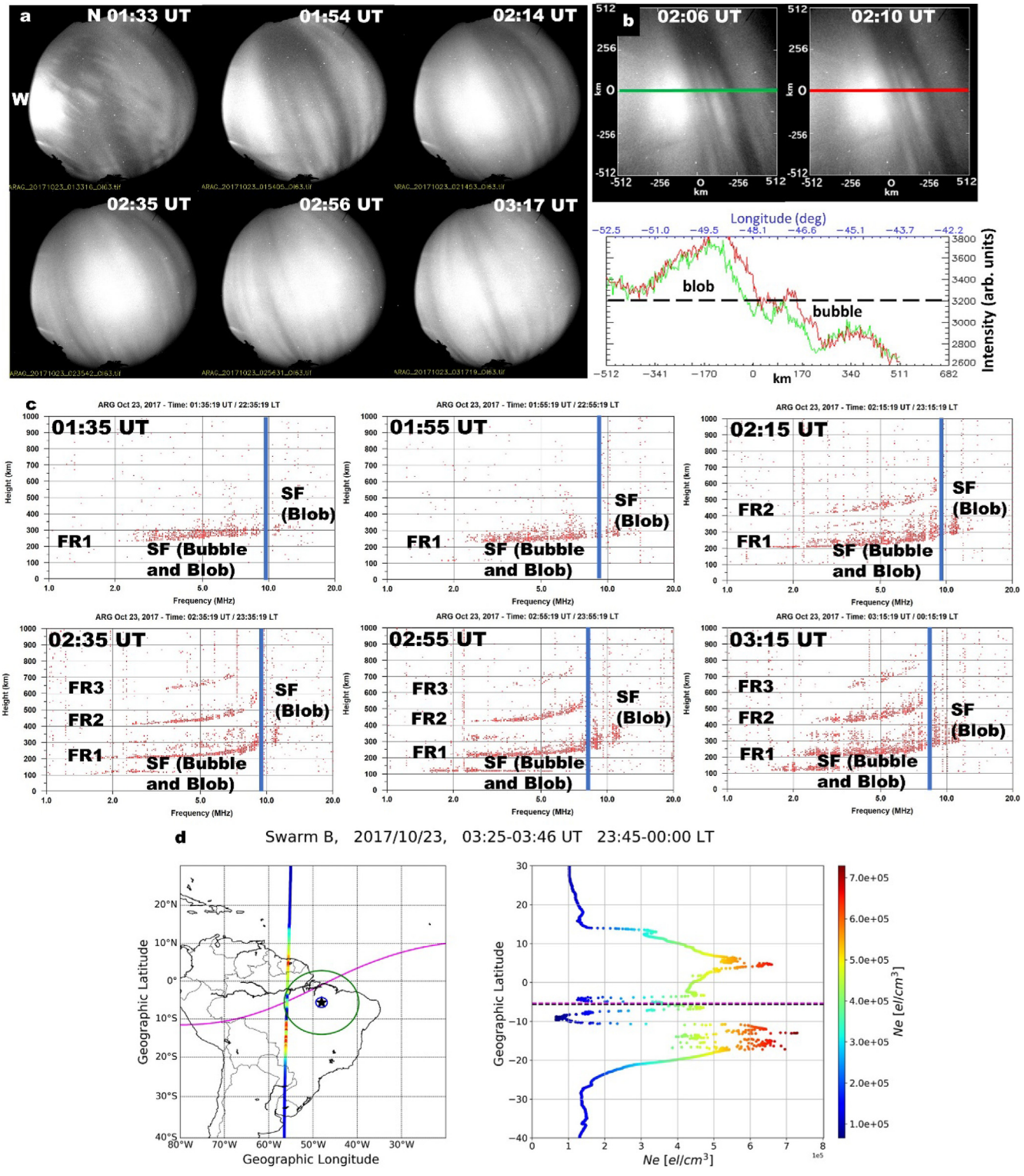

Fig. 9. Same as Fig. 7 but for the night 23 October 2017. Swarm measurements are those from Swarm B.

in the plot of Swarm A. Plasma depleted regions with respect to the background plasma density are seen at locations between the high plasma density peaks. We observe the EIA crests shifted into the northern hemisphere possibly due to due meridional winds. We also observe another high plasma density peak in the same latitude as the observation site, at the edge of the FOV of the imager system.

Table 1 gives a summary of all the nights under study listing all the occurrence times in universal time (UT) for

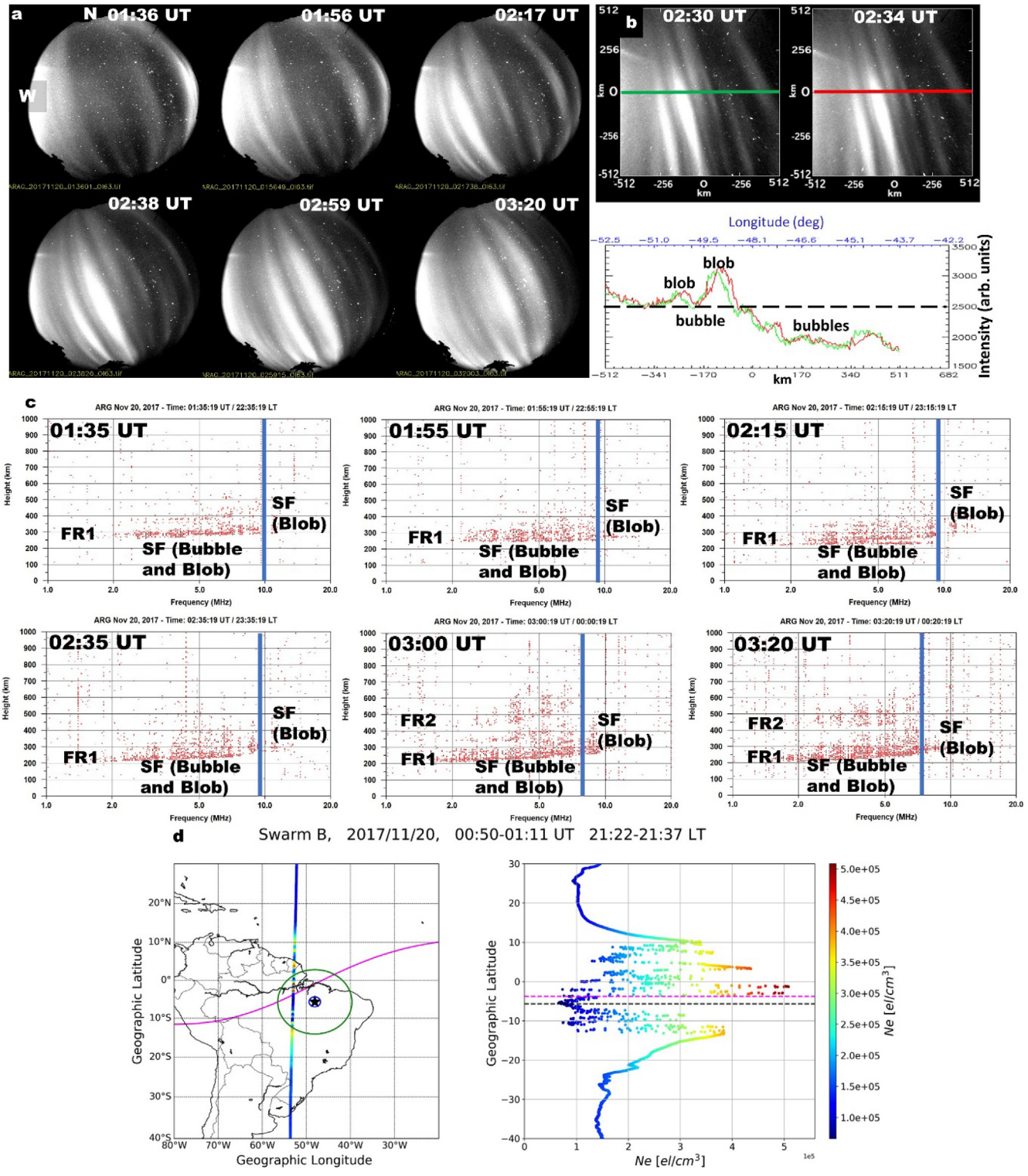

Fig. 10. Same as Fig. 7 but for the night 20 November 2017. Swarm measurements are those from Swarm B.

the structures observed by the various instruments. The times stated for the ASI and ionosonde observations are for when the structures were first observed. For the satellites, the times represent the time range within which the satellites were visible in a certain longitude. The "n/a" stands for the absence of satellite data for that night.

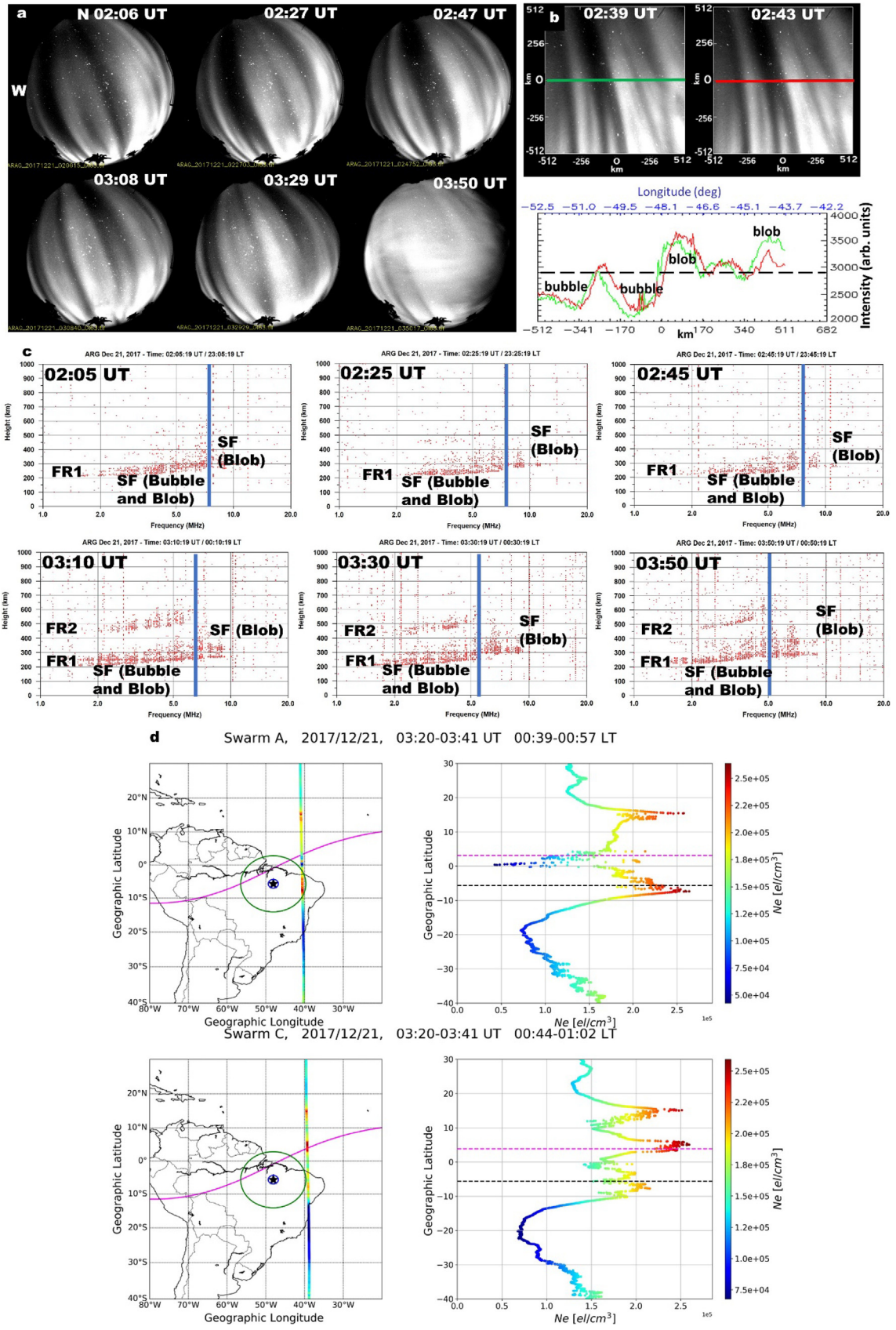

Fig. 11. Same as Fig. 7 but for the night 21 December. Swarm measurements are those from Swarm A and C.

Table 1
A summary of all observations with occurrence times in universal time (UT).

Date	ASI observations		Ionosonde observation		SWARM depletion		
	Bubbles in UT	Blobs in UT	Spread-F UT	Atypical Trace (UT)	A (UT)	B (UT)	C (UT)
07 Mar	absent	absent	absent	absent	absent	n/a	absent
29 Sep	05:02	absent	05:00	absent	n/a	04:41–05:05	n/a
14 Sep	01:02	01:43	01:20	01:43	02:07–02:28	n/a	02:07–02:28
12 Oct	00:03	00:03	00:05	00:05	n/a	03:45–04:06	n/a
21 Oct	01:04	01:24	01:05	01:25	n/a	02:28–02:49	n/a
23 Oct	01:33	01:54	01:35	01:55	n/a	03:25–03:46	n/a
20 Nov	01:36	01:56	01:35	01:55	n/a	00:50–01:11	n/a
21 Dec	01:03	01:03	01:05	01:05	03:20–03:41	n/a	03:20–03:41

5. Discussion

In the previous sections, several events of OI 630.0 nm nightglow and ionosonde observations over ARA-Brazil are presented. Six out of the eight events showed the occurrence of plasma blobs and bubbles simultaneously in the OI 630.0 nm nightglow images and atypical range ESF structures in the ionosonde observations. The different cases presented allowed to manually compare the types of traces observed in the ionograms in the absence of irregularities and when bubbles and/or bubbles appeared in the nightglow images. In-situ plasma density measurements from Swarm satellites are presented to complement the results obtained from the ground-based instruments. It is important to mention that the satellite measurements show the ionospheric conditions above the F-layer peak during the nighttime. Notwithstanding, the results from the in-situ measurements agree with the results from the ionosonde and the imager system.

In Fig. 4a, calm, background nightglow emission images in the absence of irregularities are presented. These images show no signatures of either plasma blobs or bubbles. Nightglow intensity plots also show that the plasma density in the region was uniform with no irregularities. The ionograms of the same period showed typical nighttime F-layer trace with no Spread-F structure with average background critical frequency of less than 5 MHz and the virtual height of the bottom side of ~ 200 km for the night. Meanwhile, in Fig. 5 we observe the appearance of multiple plasma bubble structures in the nightglow images. In the images we see dark bands of nightglow depleted regions, EPBs originating from the equatorward edge of the images. A confirmation of plasma depletion in the images are seen the nightglow intensity plots of Fig. 5, which show regions of low nightglow emission intensity associated with the plasma depleted areas almost aligned to the Earth' magnetic field.

The ionograms in Fig. 5c shows the occurrence of range ESFs associated with the plasma bubble. It well is known that irregularities of varied sizes cause the ESFs observed in ionograms. These irregularities can exist inside plasms bubbles, as such the occurrence of ESFs in ionograms are used as indicator for the occurrence plasma bubble. The ionograms in both events (no irregularities or waves and only plasma bubbles) show that the first and second F-layer reflections if they exist have structures that are similar in shapes as the original F-layer trace.

In section 4.3, we show different events of the appearance plasma blobs in the OI 630.0 nm nightglow images. Plasma blobs in all these events were observed alongside the plasma bubbles in the nightglow images. The plasma irregularities were observed around 01:00 UT (23:00 LT), within a latitude range of ~ 5° S to 10° S and were observed to be aligned along the magnetic field lines (Watanabe and Oya, 1986; Kil et al., 2011). The nightglow intensity plots in all the cases show regions of high and low nightglow intensities associated with regions of plasma enhancements and depletions, respectively. The generation of plasma blobs alongside plasma bubbles and their relative locations with respect to the bubbles was explained by Huang et al. (2014). They explained that depending on the development phase of plasma bubbles, blobs associated with them could be observed in different regions with respect to the bubbles, be it equatorward or poleward edge of the bubble. They continued, in the development phase, the blob can be observed above the bubble near the magnetic equator due to the uplifting of the ionosphere and, after the bubbles are fully developed, the blob is observed off the magnetic equator due to diffusion of plasma along the magnetic field lines towards the anomaly crest regions, through the fountain effect.

During **daytime hours** in quiet times, there is a vertical upward plasma drift due to the special geometric configuration resulting from the cross of the Earth's magnetic field ($\vec{B}$) and the zonal electric field ($\vec{E}$) in the near equatorial and low-latitude regions. The (almost) parallel (North-South direction) geomagnetic field to the surface of the earth at the equator and the surrounding latitudes, crossed with the daytime eastward zonal electric field yields an upward vertical drift ($\vec{E} \times \vec{B}$ upward vertical drift) of the F-layer. This causes the F-layer plasma at the equator to rise to higher altitudes and eventually deposited to low-latitude ionosphere along the geomagnetic field lines by gravitational and pressure gradient forces in a process known as the fountain effect. The results of this dislocation of plasma from the equator to the low latitudes is the formation of two crests of plasma density in the northern and

southern hemispheres between ± 15° and ± 20° dip-latitudes and a trough of low plasma at the magnetic equator. It is important to mention that the plasma density crests are created due to the removal of plasma from the geomagnetic equator to low latitudes which is different from how blobs are formed. Another point to note is that, sometimes just after sunset the zonal eastward electric field is intensified, a phenomenon called the pre-reversal enhancement electric field (PRE), which may lead to an intensification of the EIA. However, the EIA crests begin disappearing after the PRE.

The EIA is also known to exhibit local time, seasonal and solar cycle dependence (Bhuyan and Bhuyan, 2009; Mo et al., 2017). These variations leads to hemispheric asymmetry both in terms of the latitudinal location and ionization densities (Lin et al., 2007; Paul and DasGupta, 2010; Huang et al., 2013; Mo et al., 2017) and even single crests have been reported under certain conditions (Fathy and Ghamry, 2017). The hemispheric asymmetry of the EIA crest is influenced by factors like displacement of geomagnetic equator, the geomagnetic declination angle and to a large extent by the thermospheric neutral winds which transports composition, energy and momentum thereby modifying the *F region* electron density distribution around the magnetic equator producing the EIA crests (Rishbeth, 1972; Lin et al., 2007). The nature and direction of the thermospheric winds determines the intensity of the plasma density and the position of the crests in either hemisphere. For example, when the meridional thermospheric neutral winds – considered to be the primary source of interhemispheric asymmetry - blow from north to south (south - north), the plasma in the *F region* is driven upward to higher altitudes along the magnetic field lines where recombination is slower leading to higher peak plasma density in the northern (southern) hemisphere. This results in the enhancement of the ionospheric plasma as a strong equatorial fountain prevents the effect of the wind in the direction of same leaving the leeward hemisphere (Balan et al., 2018a; Balan et al., 2018b).

Even though the EIA is a typical daytime phenomenon, sometimes the post-sunset EIA crest is intensified due to PRE and since the zonal electric field reverses westward during nighttime, moving the F-layer downwards at equatorial region the EIA crests disappear after 1 or 2 h after the PRE. However, sometime the EIA can be observed late into the nighttime hours. Therefore, it is important to emphasize at this point that structures seen throughout the OI 630.0 nm nightglow images showing high OI 630.0 nm nightglow intensity emission intensities, although occurring in the nighttime could be remnants of the EIA moving plasma from the crest region to observation site which are observed as the signature of blobs.

The atypical ESF traces in Fig. 6c-11c are the ESF signatures associated with bubbles and blobs observed in the OI 630.0 nm nightglow images. In the absence of ESF, the foF2 of the ionosphere can be measured with great precision as seen as shown in section 4.1 Fig. 4c. In the typical ESFs associated with plasma bubbles only (see section 4.2 Fig. 7c), the foF2 of the ionosphere cannot be measured precisely as in section 4.1 and the trace associated with the plasma depletion and irregularities is observed at or below the critical frequency of the ionosphere. On the contrary, the atypical structures show high-frequency echoes of up to about 15 MHz on the ionograms and are observed either at or above the F layer virtual height. Sometimes, the atypical ESF is observed to separate into a typical ESF with extra structures.

The frequency associated with the blob always remained between the critical frequency and the maximum frequency for each case of atypical ESF structure presented. The irregularities moved horizontally from the west, passing overhead to the east. During the drift, the maximum frequency remained virtually unchanged. The high-plasma density structure passed overhead from west to east with little change in frequency means that the frequency of the ESF depends on the plasma densities of the irregularities and not the virtual height when they move away or to the observation site. And since plasma frequency is dependent on the square of plasma density, frequencies of ESF echoes associated with plasma bubbles are not expected to be higher than the critical frquency of the ionosphere. On the other hand, high plasma density (with irrgularities) regions assoaciated with blobs will reflect radio signals at with higher frequencies greather than the critical frequency of the background ionosphere. The high-frequency spreads observed signify that irregularities could potentially exist inside blobs just as they exist inside plasma bubbles. As such, identifying echoes (structures) at low and high frequencies on the ionograms can be the first step in distinguishing and identifying reflections from low and high plasma density regions above the observation and subsequently bubbles and blobs.

Another characteristic of the atypical ESF associated with simultaneous plasma bubbles and blobs is that the FR2 and FR3 are always different in shape and do not reach higher frequencies like the FR1. The higher-frequency part of the atypical ESF associated with the blobs do not undergo further reflections. On the contrary, in the absence of plasma blobs, the observed F-layer reflections as shown in sections 4.1 and 4.2. have shapes that are similar to the original F-layer trace the *foF2* of all the reflections are comparable. In most of the cases, we observe first the typical ESF with or without the high-frequency trace associated with the blobs. Then it develops into atypical ESF with the high-frequency trace very prominent accompanied by the FR2 and possibly FR3 traces. Then the high-frequency trace starts separating as the structure starts developing into the F-layer trace. This may indicate that the ionosonde superimposed the signatures of the bubbles and blobs in the ionograms as stated by Calvert and Cohen, (1961) ionograms are produced by scattering from individual irregularities superimposed, and in our case irregularitties from high and low plasma density region scatterers. The collocation of the ASI and the ionosonde

and simultaneous observations from these instruments provides a unique observation context to make this assumption. As such this could be a way to identify plasma blobs in ionograms when they occur in the company of plasma bubbles. And this proposed novel methodology could be especially useful in several ionospheric studies with availability of only ionosonde data. This is the second step in identifying plasma blobs using ionograms.

Narayanan et al. (2014) observed patches of ESF at frequencies higher than the background critical frequency at higher altitudes than the F-layer base height in ionograms. They suggested that these patches could be as a result of plasma blobs (enhanced plasma density) at the overhead ionosphere causing the beams to be reflected at higher frequencies. Wang et al. (2019) also reported the observation of low- and high-frequency range Spread-F over in ionograms observed over Vanimo (Papua New Guinea) and Hainan (China) and attributed them to plasma bubbles and blobs, respectively. The observed ESF at higher frequencies in ionograms due to plasma blobs by Narayanan et al. (2014) and Wang et al. (2019) are similar to the results presented in this work. Pimenta et al. (2004, 2007) observed similar Spread-F structures in ionograms in a low-latitude station at Cachoeira Paulista–Brazil, in a study using ground-based instruments and satellite data and intimated that these structures appeared in the ionograms when plasma blobs were observed in the nightglow images. The results from these studies agree with the current investigation.

These atypical spread-F structures are also similar to those reported by Fagundes et al. (2012) over Brazil using two ionosondes located in the low-latitude stations of Sao Jose dos Campos and Cachoeira Paulista. However, their report, associated the observed atypical Spread-F to MSTIDs propagating at or above the F_2-layer peak. Meanwhile, there are studies that have also linked MSTIDs to the generation of blobs using data from Swarm satellite measurements and optical/CINDI measurements (Miller et al., 2014; Kil et al. 2019). Miller et al. (2014), Kil et al. (2019) concluded that the characteristics of the observed plasma blobs were consistent with MSTID generated structures which is in line with the conclusion from Fagundes et al. (2012) that MSTIDs may have been the source of atypical ESFs observed in ionograms. This could mean a relationship between the blobs generated by the MSTIDs and the atypical ESFs as they might originate from the same source. Calvert and Cohen, (1961) in the ionograms from Huancayo at the magnetic equator observed structures like those reported in the present study. However, the origins of the structures observed by Calvert and Cohen, (1961) were linked with plasma bubbles from the midlatitudes unlike those reported by Fagundes et al. (2012) and those reported in this study.

The multi-instrument approach used here for the simultaneous observation of plasma bubbles and blobs allows for complimentary results for each instrument. The results from the Swarm satellites (Fig. 6d-11d) presented agree with those from the imager and the ionosonde. The plasma density plots show simultaneous occurrence of plasma bubbles and blobs. The high and low plasma density measurements seen in the plots are the enhanced and depleted plasma density structures observed in the OI 630.0 nm nightglow images and ionograms. Most of the plasma density plots showed plasma density fluctuations inside the density maxima and minima corresponding to bubbles and blobs. This agrees with the high- and low- frequency range spreads associate with plasma blobs and bubbles in the ionograms. This shows that plasma blobs, like bubbles, could contain irregularities. Again, in most cases, two peaks of enhanced electron density in the northern and southern hemisphere and depleted plasma densities around the equatorial region except in the first case where peak plasma density was observed in the southern hemisphere (Xiong et al., 2018; Kil et al., 2019). According to Kil et al. (2019), meridional winds which changes and introduces asymmetry in the EIA structure may be responsible for the modification of the plasma blobs and as such might have partly increased the plasma density in the observation area thereby being a possible source of the occurrence of plasma bubbles in the low-latitude, equatorial region. It must be noted that the results from the two Swarm satellites (A and C) present variations in the structures and their locations. This may be because of the difference in the local times due to the longitudinal separation between Swarm A and C.

Le et al. (2003) observed plasma blobs in the EIA crest region alongside plasma bubbles and near the magnetic equator and explained that during the upward motion of plasma bubble, the field-aligned plasma pressure gradient at the poleward edges of plasma depletions produces an equatorward force that drives the plasma particles to the equator. This force restricts the density depletions to the anomaly crests region preventing them from extending to higher latitudes. As such the polarization electric fields which are inside the depletion region can be mapped to higher latitudes and move the high-density plasma near the anomaly crest to increase plasma density just above the flux tubes. This explanation was supported by simulations from Krall et al. (2010) and observations from Pimenta et al. (2004), Tardelli-Coelho et al. (2017). It shows that plasma blobs occur at the poleward edges EPBs. However, Huang et al. (2014) and Wang et al. (2019) have reported the observations of plasma blobs at the equatorward edges of EPBs. According to Huang et al. (2014), the location of plasma blobs (equatorward/poleward edge) with respect to plasma bubbles depends on the evolution stage of the bubbles and that the polarization electric field inside the EPBs moves plasma upward and causes blobs to form above the EPBs in the intermediate stage of the bubble's evolution.

6. Conclusions

In this study, we have presented simultaneous observation of plasma bubbles and blobs in OI 630.0 nm nightglow images and atypical range Spread-F in ionograms. The unique advantage of having a collocated imaging system and ionosonde coupled with simultaneous observations allowed us to present a novel methodology to identify plasma blobs in ionograms when they occur in the company of plasma bubbles. The ability to identify the signature of blobs in ionograms will allow for the study of blobs without simultaneous all-sky OI 630.0 nm observations considering that ionosonde observations are not limited by weather or moonlight conditions like in the case of the imaging systems. The results are as below.

1. Plasma blobs observed in OI 630.0 nm nightglow images are accompanied by high-frequency atypical ESF echoes, in ionograms, with frequencies reaching up to ~15 MHz or higher.
2. The frequencies of the atypical ESFs observed in the ionograms associated with the plasma bubble/blob pairs are mostly greater than the background critical frequency.
3. The first F-layer reflections observed when there is atypical ESF is different in shape from the second, third and higher order reflections.
4. Higher frequencies are not reflected when blobs appear such that the first reflection echoes reach higher frequencies than subsequent reflections. This could mean that when plasma bubbles and blobs occur simultaneously, the signatures are superimposed on each other. This is not observed when only bubbles occur or in the absence of blobs.
5. The blobs just like bubbles could contain irregularities observed as range echoes in the higher-frequency portion of the atypical ESF.

Declaration of Competing Interest

The authors declare that they have no known competing financial interests or personal relationships that could have appeared to influence the work reported in this paper.

Acknowledgements

The authors wish to express their sincere gratitude to the Fundação de Amparo a Pesquisa do Estado de Sao Paulo (FAPESP), for providing financial support through the process № 2012/08445-9. This study was financed in part by the "Coordenação de Aperfeiçoamento de Pessoal de Nível Superior – Brasil (CAPES)". The Conselho Nacional de Desenvolvimento Científico e Tecnológico (CNPq) through grant 302406/2017-4 and FINEP № 01.100661-00 for the partial financial support. One of the Authors (KV) wish to express his sincere thanks to National Atmospheric Research Laboratory (NARL) for providing fellowship.

Data availability

The nightglow and ionogram data used in this manuscript are accessible at http://www1.univap.br/ionosfera/Paper_Data/Ebenezer_2019.zip and the Swarm data can be obtained from https://swarm-diss.eo.esa.int/ or specifically from ftp://swarm-diss.eo.esa.int/Level1b/Latest_baselines/EFIx_LP/

Authors' contribution

EA-Y did the data analysis and wrote majority of the manuscript. PRF supervised the development of the work and helped to write the manuscript. GVP, AT, KV, FO designed the experiment and/or coordinated the observations. MP and AP analyzed the Satellite data. All authors contributed to the manuscript by correcting and suggesting new insights.

References

Alfonsi, L., Spogli, L., Pezzopane, M., Romano, V., Zuccheretti, E., De Franceschi, G., Cabrera, M.A., Ezquer, R.G., 2013. Comparative analysis of spread-F signature and GPS scintillation occurrences at Tucumán. Argentina. J. Geophys. Res. Sp. Phys. 118 (7), 4483–4502. https://doi.org/10.1002/jgra.50378.

Balan, N., Liu, L., Le, H., 2018a. A brief review of equatorial ionization anomaly and ionospheric irregularities. Earth Planet. Phys. 2, 1–19 https://doi.org/10.26464/epp2018025.

Balan, N., Souza, J., Bailey, G.J., 2018b. Recent developments in the understanding of equatorial ionization anomaly: A review. J. Atmos. Solar-Terrestrial Phys. 171, 3–11. https://doi.org/10.1016/j.jastp.2017.06.020.

Bhuyan, P.K., Bhuyan, K., 2009. The equatorial ionization anomaly at the topside F region of the ionosphere along 75°E. Adv. Sp. Res. 43 (11), 1676–1682. https://doi.org/10.1016/j.asr.2008.09.027.

Calvert, W., Cohen, R., 1961. The interpretation and synthesis of certain spread- F configurations appearing on equatorial ionograms. J. Geophys. Res. 66 (10), 3125–3140. https://doi.org/10.1029/JZ066i010p03125.

Cherniak, I., Zakharenkova, I., 2016. First observations of super plasma bubbles in Europe. Geophysical Research Letters 43 (21), 11,137–11,145. https://doi.org/10.1002/2016GL071421.

Fagundes, P.R., Bittencourt, J.A., de Abreu, A.J., Moor, L.P., Muella, M. T.A.H., Sahai, Y., Abalde, J.R., Pezzopane, M., Sobral, J.H.A., Abdu, M.A., Pimenta, A.A., Amorim, D.C.M., 2012. Atypical nighttime spread-F structure observed near the southern crest of the ionospheric equatorial ionization anomaly. J. Geophys. Res. Sp. Phys. 117, 1–9. Phys. 117 (A4), n/a–n/a. https://doi.org/10.1029/2011JA017118.

Fathy, A., Ghamry, E., 2017. A statistical study of single crest phenomenon in the equatorial ionospheric anomaly region using Swarm A satellite. Adv. Sp. Res. 59 (6), 1539–1547. https://doi.org/10.1016/j.asr.2016.12.020.

Friis-Christensen, E., Lühr, H., Hulot, G., 2006. Swarm: A constellation to study the Earth's magnetic field. Earth, Planets Space 58, 351–358. https://doi.org/10.1186/BF03351933.

Friis-Christensen, E., Lühr, H., Knudsen, D., Haagmans, R., 2008. Swarm – An Earth Observation Mission investigating Geospace. Advances in Space Research 41 (1), 210–216. https://doi.org/10.1016/j.asr.2006.10.008.

Huang, L., Huang, J., Wang, J., Jiang, Y., Deng, B., Zhao, K., Lin, G., 2013. Analysis of the north-south asymmetry of the equatorial

ionization anomaly around 110°E longitude. J. Atmos. Solar-Terrestrial Phys. 102, 354–361. https://doi.org/10.1016/j.jastp.2013.06.010.
Huang, L., Wang, J., Jiang, Y., Huang, J., Chen, Z., Zhao, K., 2014. A preliminary study of the single crest phenomenon in total electron content (TEC) in the equatorial anomaly region around 120°E longitude between 1999 and 2012. Adv. Sp. Res. 54 (11), 2200–2207. https://doi.org/10.1016/j.asr.2014.08.021.
Kil, H., Choi, H.-S., Heelis, R.A., Paxton, L.J., Coley, W.R., Miller, E.S., 2011. Onset conditions of bubbles and blobs: A case study on 2 March 2009. Geophys. Res. Lett. 38 (6), n/a–n/a. https://doi.org/10.1029/2011GL046885.
Kil, H., Paxton, L.J., Jee, G., Nikoukar, R., 2019. Plasma Blobs Associated With Medium-Scale Traveling Ionospheric Disturbances. Geophys. Res. Lett. 46 (7), 3575–3581. https://doi.org/10.1029/2019GL082026.
Krall, J., Huba, J.D., Joyce, G., Yokoyama, T., 2010. Density enhancements associated with equatorial spread F. Ann. Geophys. 28, 327–337. https://doi.org/10.5194/angeo-28-327-2010 https://doi.org/10.1029/2002JA009592.
Kumar, S., 2017. Morphology of equatorial plasma bubbles during low and high solar activity years over Indian sector. Astrophysics and Space Science 362 (5). https://doi.org/10.1007/s10509-017-3074-3.
Le, G., Huang, C.S., Pfaff, R.F., Su, S.Y., Yeh, H.C., Heelis, R.A., Rich, F.J., Hairston, M., 2003. Plasma density enhancements associated with equatorial spread F: ROCSAT-1 and DMSP observations. J. Geophys. Res. Sp. Phys. 108, 1–14. https://doi.org/10.1029/2002JA009592.
Lin, C.H., Liu, J.Y., Fang, T.W., Chang, P.Y., Tsai, H.F., Chen, C.H., Hsiao, C.C., 2007. Motions of the equatorial ionization anomaly crests imaged by FORMOSAT-3/COSMIC. Geophys. Res. Lett. 34, 1–6. https://doi.org/10.1029/2007GL030741.
McNamara, L.F., Caton, R.G., Parris, R.T., Pedersen, T.R., Thompson, D.C., Wiens, K.C., Groves, K.M, 2013. Signatures of equatorial plasma bubbles in VHF satellite scintillations and equatorial ionograms. Radio Science 48 (2), 89–101. https://doi.org/10.1002/rds.20025.
Mendillo, M., Baumgardner, J., 1982. Airglow characteristics of equatorial plasma depletions. J. Geophys. Res. 87, 7641. https://doi.org/10.1029/2007GL030741.
Miller, E.S., Kil, H., Makela, J.J., Heelis, R.A., Talaat, E.R., Gross, A., 2014. Topside signature of medium-scale traveling ionospheric disturbances. Ann. Geophys. 32, 959–965. https://doi.org/10.1029/2007GL030741.
Mo, XiaoHua, Zhang, DongHe, Goncharenko, L., Zhang, ShunRong, Hao, YongQiang, Xiao, Z., Pei, JiaZheng, Yoshikawa, A., Chau, HaDuyen, 2017. Meridional movement of northern and southern equatorial ionization anomaly crests in the East-Asian sector during 2002–2003 SSW. Sci. China Earth Sci. 60 (4), 776–785. https://doi.org/10.1007/s11430-016-0096-y.
Narayanan, V.L., Sau, S., Gurubaran, S., Shiokawa, K., Balan, N., Emperumal, K., Sripathi, S., 2014. A statistical study of satellite traces and evolution of equatorial spread F Space science. Earth, Planets Sp. 66, 1–13. https://doi.org/10.1186/s40623-014-0160-4.
OYA, H., TAKAHASHI, T., WATANABE, S., 1986. Observation of Low Latitude Ionosphere by the Impedance Probe on Board the Hinotori Satellite. J. Geomagn. Geoelectr. 38 (2), 111–123. https://doi.org/10.5636/jgg.38.111.
Park, J., Lühr, H., Michaelis, I., Stolle, C., Rauberg, J., Buchert, S., Reine, G., Merayo, Jose M.G., Brauer, P., 2015. Westward tilt of low-latitude plasma blobs as observed by the Swarm constellation. Journal of Geophysical Research: Space Physics 120 (4), 3187–3197. https://doi.org/10.1002/2014JA020965.
Park, J., Min, K.W., Lee, J.J., Kil, H., Kim, V.P., Kim, H.J., Lee, E., Lee, D.Y., 2003. Plasma blob events observed by KOMPSAT-1 and DMSP F15 in the low latitude nighttime upper ionosphere. Geophys. Res. Lett. 30, 2–5. https://doi.org/10.1029/2003GL018249.
Paul, A., DasGupta, A., 2010. Characteristics of the equatorial ionization anomaly in relation to the day-to-day variability of ionospheric irregularities around the postsunset period. Radio Sci. 45 (6), n/a–n/a. https://doi.org/10.1029/2009RS004329.
Paulino, I., Medeiros, A.F., Buriti, R.A., Sobral, J.H.A., Takahashi, H., Gobbi, D., 2010. Optical observations of plasma bubble westward drifts over Brazilian tropical region. J. Atmos. Solar-Terrestrial Phys. 72 (5-6), 521–527. https://doi.org/10.1016/j.jastp.2010.01.015.
Pezzopane, M., Pignalberi, A., 2019. The ESA Swarm mission to help ionospheric modeling: a new NeQuick topside formulation for mid-latitude regions. Scientific Reports 9 (12253). https://doi.org/10.1038/s41598-019-48440-6.
Pillat, V.G., Fagundes, P.R., Guimarães, L.N.F., 2015. Automatically identification of Equatorial Spread-F occurrence on ionograms. J. Atmos. Solar-Terrestrial Phys. 135, 118–125. https://doi.org/10.1016/j.jastp.2015.10.015.
Pimenta, A.A., Fagundes, P.R., Bittencourt, J.A., Sahai, Y., Gobbi, D., Medeiros, A.F., Taylor, M.J., Takahashi, H., 2001. Ionospheric plasma bubble zonal drift: A methodology using OI 630 mn all-sky imaging systems. Adv. Sp. Res. 27, 1219–1224. https://doi.org/10.1016/S0273-1177(01)00201-0.
Pimenta, A.A., Sahai, Y., Bittencourt, J.A., Abdu, M.A., Takahashi, H., Taylor, M.J., 2004. Plasma blobs observed by ground-based optical and radio techniques in the Brazilian tropical sector. Geophys. Res. Lett. 31 (12), n/a–n/a. https://doi.org/10.1029/2004GL020233.
Pimenta, A.A., Sahai, Y., Bittencourt, J.A., Rich, F.J., 2007. Ionospheric plasma blobs observed by OI 630 nm all-sky imaging in the Brazilian tropical sector during the major geomagnetic storm of April 6–7, 2000. Geophys. Res. Lett. 34, 1–5. https://doi.org/10.1029/2006GL028529.
Rishbeth, H., 1972. Thermospheric winds and the F-region: A review. J. Atmos. Terr. Phys. 34 (1), 1–47. https://doi.org/10.1016/0021-9169(72)90003-7.
Sahai, Y., Fagundes, P.R., Bittencourt, J.A., 2000. Transequatorial F-region ionospheric plasma bubbles: solar cycle effects. J. Atmos. Solar-Terrestrial Phys. 62 (15), 1377–1383. https://doi.org/10.1016/S1364-6826(00)00179-6.
Sobral, J.H.A., Abdu, M.A., Takahashi, H., Taylor, M.J., De Paula, E.R., Zamlutti, C.J., De Aquino, M.G., Borba, G.L., 2002. Ionospheric plasma bubble climatology over Brazil based on 22 years (1977–1998) of 630 nm airglow observations. J. Atmos. Solar-Terrestrial Phys. 64, 1517–1524. https://doi.org/10.1016/S1364-6826(00)00179-6.
Sobral, J.H.A., de Castilho, V.M., Abdu, M.A., Takahashi, H., Paulino, I., Gasparelo, U.A.C., Arruda, D.C.S., Mascarenhas, M., Zamlutti, C. J., Denardini, C.M., Koga, D., de Medeiros, A.F., Buriti, R.A., 2011. Midnight reversal of ionospheric plasma bubble eastward velocity to westward velocity during geomagnetically quiettime: Climatology and its model validation. J. Atmos. Solar-Terrestrial Phys. 73 (11-12), 1520–1528. https://doi.org/10.1016/j.jastp.2010.11.031.
Tardelli-Coelho, F., Pimenta, A.A., Tardelli, A., Abalde, J.R., Venkatesh, K., 2017. Plasma blobs associated with plasma bubbles observed in the Brazilian sector. Adv. Sp. Res. 60 (8), 1716–1724. https://doi.org/10.1016/j.asr.2017.06.018.
Wang, Z., Liu, H., Shi, J., Wang, G., Wang, X., 2019. Plasma Blobs Concurrently Observed With Bubbles in the Asian-Oceanian Sector During Solar Maximum. J. Geophys. Res. Sp. Phys. 124 (8), 7062–7071. https://doi.org/10.1029/2018JA026373.
Yokoyama, T., Su, S.Y., Fukao, S., 2007. Plasma blobs and irregularities concurrently observed by ROCSAT-1 and Equatorial Atmosphere Radar. Journal of Geophysical Research: Space Physics 112 (5), 1–7. https://doi.org/10.1029/2006JA012044.
Watanabe, S., Oya, H., 1986. Occurrence characterisrics of low latitude ionosphere Irregualrities observed by impedance probe on board the Hinotori satellite 125–149. https://doi.org/10.5636/jgg.38.125
Xiong, C., Xu, J., Wu, K., Yuan, W., 2018. Longitudinal Thin Structure of Equatorial Plasma Depletions Coincidently Observed by Swarm Constellation and all-Sky Imager. J. Geophys. Res. Sp. Phys. 123 (2), 1593–1602. https://doi.org/10.1002/2017JA025091.